

1 **Systematic and Objective Evaluation of Earth System Models: PCMDI**  
2 **Metrics Package (PMP) version 3**

3  
4 Jiwoo Lee<sup>1</sup>, Peter J. Gleckler<sup>1</sup>, Min-Seop Ahn<sup>2,3</sup>, Ana Ordonez<sup>1</sup>, Paul A. Ullrich<sup>1,4</sup>, Kenneth R.  
5 Sperber<sup>1,a</sup>, Karl E. Taylor<sup>1</sup>, Yann Y. Planton<sup>5,6</sup>, Eric Guilyardi<sup>7,8</sup>, Paul Durack<sup>1</sup>, Celine Bonfils<sup>1</sup>,  
6 Mark D. Zelinka<sup>1</sup>, Li-Wei Chao<sup>1</sup>, Bo Dong<sup>1</sup>, Charles Doutriaux<sup>1</sup>, Chengzhu Zhang<sup>1</sup>, Tom Vo<sup>1</sup>,  
7 Jason Boutte<sup>1</sup>, Michael F. Wehner<sup>9</sup>, Angeline G. Pendergrass<sup>10,11</sup>, Daehyun Kim<sup>12</sup>, Zeyu Xue<sup>13</sup>,  
8 Andrew T. Wittenberg<sup>14</sup>, and John Krasting<sup>14</sup>

9  
10 <sup>1</sup> Lawrence Livermore National Laboratory, Livermore, California, USA

11 <sup>2</sup> NASA Goddard Space Flight Center, Greenbelt, MD, USA

12 <sup>3</sup> ESSIC, University of Maryland, College Park, MD, USA

13 <sup>4</sup> University of California, Davis, Davis, California, USA

14 <sup>5</sup> NOAA Pacific Marine Environmental Laboratory, Seattle, Washington, USA

15 <sup>6</sup> Monash University, Clayton, Australia

16 <sup>7</sup> LOCEAN-IPSL, CNRS-IRD-MNHN-Sorbonne Université, Paris, France

17 <sup>8</sup> National Centre for Atmospheric Science-Climate, University of Reading, Reading, UK

18 <sup>9</sup> Lawrence Berkeley National Laboratory, Berkeley, California, USA

19 <sup>10</sup> Department of Earth and Atmospheric Science, Cornell University, Ithaca, New York, USA

20 <sup>11</sup> National Center for Atmospheric Research, Boulder, Colorado, USA

21 <sup>12</sup> School of Earth and Environmental Sciences, Seoul National University, Seoul, South Korea

22 <sup>13</sup> Pacific Northwest National Laboratory, Richland, WA, USA

23 <sup>14</sup> NOAA Geophysical Fluid Dynamics Laboratory, Princeton, NJ, USA

24 <sup>a</sup> Retired

25  
26 Submitted to [Geosic. Model Dev. \(GMD\)](#) in November 2023

27 Revised in December 2023

28 Second Revised in March 2024

29  
30 *Corresponding to:* Jiwoo Lee ([lee1043@llnl.gov](mailto:lee1043@llnl.gov))

31 7000 East Ave, Livermore, California 94550, USA

32 **Abstract**

33

34 Systematic, routine, and comprehensive evaluation of Earth System Models (ESMs) facilitates benchmarking  
35 improvement across model generations and identifying the strengths and weaknesses of different model  
36 configurations. By gauging the consistency between models and observations, this endeavor is becoming increasingly  
37 necessary to objectively synthesize thousands of simulations contributed to the Coupled Model Intercomparison  
38 Project (CMIP) to date. The Program for Climate Model Diagnosis and Intercomparison (PCMDI) Metrics Package  
39 (PMP) is an open-source Python software package that provides "quick-look" objective comparisons of ESMs with  
40 one another and with observations. The comparisons include metrics of large- to global-scale climatologies, tropical  
41 inter-annual and intra-seasonal variability modes such as El Niño-Southern Oscillation (ENSO) and Madden-Julian  
42 Oscillation (MJO), extratropical modes of variability, regional monsoons, cloud radiative feedbacks, and high-  
43 frequency characteristics of simulated precipitation, including its extremes. The PMP comparison results are produced  
44 using all model simulations contributed to CMIP6 and earlier CMIP phases. An important objective of the PMP is to  
45 document performance of ESMs participating in the recent phases of CMIP, together with providing version-  
46 controlled information for all data sets, software packages, and analysis codes being used in the evaluation process.  
47 Among other purposes, this also enables modeling groups to assess performance changes during the ESM development  
48 cycle in the context of the error distribution of the multi-model ensemble. Quantitative model evaluation provided by  
49 the PMP can assist modelers in their development priorities. In this paper, we provide an overview of the PMP  
50 including its latest capabilities, and discuss its future direction.

## 51 **1 Introduction**

52 Earth System Models (ESMs) are key tools for projecting climate change and conducting research to enhance  
53 our understanding of the Earth system. With the advancements in computing power and the increasing importance of  
54 climate projections, there has been an exponential growth of diversity of ESM simulations. During the 1990's, the  
55 Atmospheric Model Intercomparison Project (AMIP; Gates, 1992; Gates et al., 1999) was a centralizing activity within  
56 the modeling community, which led to the creation of the Coupled Model Intercomparison Project (CMIP; Meehl et  
57 al., 1997, 2000, 2007; Covey et al., 2003; Taylor et al., 2012). Since 1989, the Program for Climate Model Diagnosis  
58 and Intercomparison (PCMDI) has worked closely with the World Climate Research Programme's (WCRP) Working  
59 Group on Coupled Models (WGCM) and Working Group on Numerical Experimentation (WGNE) to design and  
60 implement these projects (Potter et al., 2011). The most recent phase of CMIP (CMIP6; Eyring et al., 2016) provides  
61 a set of well-defined experiments that most climate modeling centers perform, and subsequently makes results  
62 available for a large and diverse community to analyze.

63 Evaluating ESMs is a complex endeavor, given the vast range of climate characteristics across space and  
64 time scales. A necessary step involves quantifying the consistency between ESMs with available observations. Climate  
65 model performance metrics have been widely used to objectively and quantitatively gauge the agreement between  
66 observations and simulations to summarize model behavior with a wide range of climate characteristics. Simple  
67 examples include either the model bias or the pattern similarity (correlation) between an observed and simulated field  
68 (e.g., Taylor, 2001). With the rapid growth in the number, scale, and complexity of simulations, the metrics have been  
69 used more routinely as exemplified by the Intergovernmental Panel on Climate Change (IPCC) Assessment Reports  
70 (e.g., Gates et al., 1995; McAvaney et al., 2001; Randall et al., 2007; Flato et al., 2014; Eyring et al., 2021). A few  
71 studies have been exclusively devoted to objective model performance assessment using summary statistics. Lambert  
72 and Boer (2001) evaluated the first set of CMIP models from CMIP1 using statistics for the large-scale mean climate.  
73 Gleckler et al. (2008) identified a variety of factors relevant to model metrics and demonstrated techniques to quantify  
74 the relative strengths and weaknesses of the simulated mean climate. Reichler and Kim (2008) attempted to gauge  
75 model improvements across the early phases of CMIP. The scope of objective model evaluation has greatly broadened  
76 beyond the mean state in recent years (e.g., Gleckler et al., 2016; Eyring et al., 2019), including attempts to establish  
77 performance metrics for a wide range of climate variability (e.g., Kim et al., 2009; Sperber et al., 2013; Ahn et al.,  
78 2017; Fasullo et al., 2020; Lee et al., 2021b; Planton et al., 2021) and extremes (e.g., Sillmann et al., 2013; Srivastava  
79 et al., 2020; Wehner et al., 2020, 2021). Guilyardi et al. (2009) and Reed et al. (2022) emphasized that metrics should  
80 be concise, interpretable, informative, and intuitive.

81 With the growth of data size and diversity of ESM simulations, there has been a pressing need for the research  
82 community to become more efficient and systematic in evaluating ESMs and documenting their performances. To  
83 respond to the need, PCMDI developed the PCMDI Metrics Package (PMP) and released its first version in 2015 (see  
84 Code and Data Availability section for all versions). A centralizing goal of the PMP then and now is to quantitatively  
85 synthesize results from the archive of CMIP simulations via performance metrics that help characterize the overall  
86 agreement between models and observations (Gleckler et al., 2016). For our purposes, "performance metrics" are  
87 typically (but not exclusively) well-established statistical measures that quantify the consistency between observed

88 and simulated characteristics. Common examples include a domain average bias, a root-mean-square error (RMSE),  
89 a spatial pattern correlation, or others, typically selected depending on the application. Another goal of the PMP is to  
90 further diversify the suite of high-level performance tests that help characterize the simulated climate. The results  
91 provided by the PMP are frequently used to address two overarching and recurring questions: 1) What are the relative  
92 strengths and weaknesses between different models? and 2) How are models improving with further development?  
93 Addressing the second question is often referred to as “benchmarking” and this motivates an important emphasis of  
94 the effort described in this paper—striving to advance the documentation of all data and results of the PMP in an open  
95 and ultimately reproducible manner.

96 In parallel, the current progress towards systematic model evaluation remains dynamic, with evolving  
97 approaches and many independent paths being pursued. This has resulted in the development of diversified model  
98 evaluation software packages. Examples in addition to the PMP include the ESMValTool (Eyring et al., 2016, 2019,  
99 2020; Righi et al., 2020), the Model Diagnostics Task Force (MDTF) Diagnostics package (Maloney et al., 2019;  
100 Neelin et al., 2023), the International Land Model Benchmarking (ILAMB) Software System (Collier et al., 2018) that  
101 focuses on land surface and carbon cycle metrics, and the International Ocean Model Benchmarking (IOMB) Software  
102 System (Fu et al., 2022) that focuses on surface and upper ocean biogeochemical variables. Some tools have been  
103 developed with a more targeted focus on a specific subject area, such as the Climate Variability Diagnostics Package  
104 (CVDP) that diagnoses climate variability modes (Phillips et al., 2014; Fasullo et al., 2020), and the Analyzing Scales  
105 of Precipitation (ASoP) that focuses on analyzing precipitation scales across space and time (Klingaman et al., 2017;  
106 Martin et al., 2017; Ordonez et al., 2021). The regional climate community also has actively developed metrics  
107 packages such as the Regional Climate Model Evaluation System (RCMES; Lee et al., 2018a). Separately, a few  
108 climate modeling centers have developed their own model evaluation packages to assist in their in-house ESM  
109 development, e.g., the E3SM Diags (Zhang et al., 2022). There also have been other efforts to enhance the usability  
110 of in-situ and field campaign observations in ESM evaluations, such as Atmospheric Radiation Measurement (ARM)  
111 GCM Diag (Zhang et al., 2018, 2020) and Earth System Model Aerosol–Cloud Diagnostics (ESMAC Diags; Tang et  
112 al., 2022, 2023). While they all have their own scientific priorities and technical approaches, the uniqueness of the  
113 PMP is its focus on the objective characterization of the physical climate system as simulated by community models.  
114 An important prioritization of the PMP is to advance all aspects of its workflow, in an open, transparent, and  
115 reproducible manner, which is critical for benchmarking. The PMP summary statistics characterizing CMIP  
116 simulations are version-controlled and made publicly available as a resource to the community.

117 In this paper, we describe the latest update of the PMP and its focus on providing a diverse suite of summary  
118 statistics that can be used to construct “quick-look” summaries of ESM performance from simulations made publicly  
119 available to the research community, notably CMIP. The rest of the paper is organized as follows. In Sect. 2, we  
120 provide a technical description of the PMP and its accompanying reference datasets. In Sect. 3, we describe various  
121 sets of simulation metrics that provide an increasingly comprehensive portrayal of physical processes across time  
122 scales ranging from hours to centurial. In Sect. 4, we introduce the usage of PMP for model benchmarking. We discuss  
123 the future direction and the remaining challenges in Sect. 5 and conclude with a summary in Sect. 6. To assist the  
124 reader, the table in Appendix A summarizes the acronyms used in this paper.

125

## 126 2 Software package and data description

127 The PMP is a Python-based open-source software framework ([https://github.com/PCMDI/pcmdi\\_metrics](https://github.com/PCMDI/pcmdi_metrics))  
128 designed to objectively gauge the consistency between ESMs and available observations via well-established statistics  
129 such as those discussed in Sect. 3. The PMP has been mainly used for the evaluation of CMIP-participating models.  
130 A subset of CMIP experiments, those conducted using the observation forcings such as “Historical” and “AMIP”  
131 (Eyring et al., 2016), is particularly well suited for comparing models with observations. The AMIP experiment  
132 protocol constrains the simulation with prescribed sea surface temperature (SST), and the “Historical” experiment is  
133 conducted using coupled model simulations driven by observed varying natural and anthropogenic forcings. Some of  
134 the metrics applicable to these experiments may also be relevant to others (e.g., multi-century coupled control runs  
135 called “PiControl” and idealized “4xCO2” simulations that are designed for estimating climate sensitivity).

136 The PMP has been applied to multiple generations of CMIP models in a quasi-operational fashion as new  
137 simulations are made available, new analysis methods are incorporated, or new observational data become accessible  
138 (e.g., Gleckler et al. 2016; Planton et al., 2021; Lee et al., 2021b; Ahn et al. 2022). Shortly after simulations from the  
139 most recent phase of the CMIP (i.e., CMIP6) became accessible, PMP quick-look summaries were provided on the  
140 PCMDI’s website (<https://pcmdi.llnl.gov/metrics/>), offering a resource to scientists involved in CMIP or others  
141 interested in the evaluation of ESMs. To facilitate this, at PCMDI the PMP is technically linked to the Earth System  
142 Grid Federation (ESGF) that is the CMIP data delivery infrastructure (Williams et al., 2016).

143 The primary deliverable of the PMP is a collection of summary statistics. We strive to make the baseline  
144 results (raw statistics) publicly available and well-documented, and continue to make advances with this objective in  
145 priority. For our purposes, we are referring to model performance “summary statistics” and “metrics” interchangeably,  
146 although in some situations we consider there to be an important distinction. For us, a genuine performance metric  
147 constitutes a well-defined and established statistic that has been used in a very specific way (e.g., a particular variable,  
148 analysis, and domain) for long-term benchmarking (see Sect. 4). The distinction between summary statistics and  
149 metrics is application-dependent and evolving as the community advances efforts to establish quasi-operational  
150 capabilities to gauge ESM performance. Some visualization capabilities described in Sect. 3 are made available  
151 through the PMP. Users can also further explore the model data comparisons using their preferred visualization  
152 methods or incorporate the results into their own studies from the summary statistics from the PMP. Noting the above,  
153 the scope of the PMP is fairly targeted. It is not intended to be “all-purpose”, e.g. by incorporating the vast range of  
154 diagnostics used in model evaluation.

155 The PMP is designed to readily work with model output that has been processed using the Climate Model  
156 Output Rewriter (CMOR; <https://cmor.llnl.gov/>), which is a software library developed to prepare model output  
157 following the CF Metadata Conventions (Hassell et al., 2017; Eaton et al., 2022, <http://cfconventions.org/>) in Network  
158 Common Data Form (NetCDF) format. The CMOR is used by most modeling groups contributing to CMIP, ensuring  
159 all model output adheres to the CMIP data structures that themselves are based on the CF conventions. It is possible  
160 to use the PMP on model output that has not been prepared by CMOR, but this usually requires additional work, e.g.,  
161 mapping the data to meet the community standards.

162 For reference datasets, the PMP uses observational products processed to be compliant with the Observations  
163 for Model Intercomparison Projects (obs4MIPs; <https://pcmdi.github.io/obs4MIPs/>). The obs4MIPs effort was  
164 initiated circa 2010 (Gleckler et al., 2011) to advance the use of the observations in model evaluation and research.  
165 Substantial progress has been made in establishing obs4MIPs data standards that technically align with CMIP model  
166 output (e.g., Teixeira et al., 2014; Ferraro et al., 2015), with the data products published on the ESGF (Waliser et al.,  
167 2020). Obs4MIPs-compliant data were prepared with CMOR, and the data directly available via obs4MIPs are used  
168 as PMP reference datasets.

169 The PMP leverages other Python-based open-source tools and libraries such as *xarray* (Hoyer and Hamman,  
170 2017), *eofs* (Dawson, 2016), and many others. One of the primary fundamental tools used in the latest PMP version  
171 is the Python package, Xarray Climate Data Analysis Tools (xCDAT; Vo et al., 2023; <https://xcdat.readthedocs.io>).  
172 The xCDAT is developed to provide a more efficient, robust, and streamlined user experience in climate data analysis  
173 when using *xarray* (<https://docs.xarray.dev/>). Portions of the PMP rely on the precursor of the xCDAT, a Python  
174 library called Community Data Analysis Tools (CDAT, Williams et al., 2009; Williams, 2014; Doutriaux et al., 2019),  
175 which has been fundamental since the early development stages of the PMP. The *xarray* software provides much of  
176 the functionality of CDAT (e.g., I/O, indexing, and subsetting). However, it lacks some key climate domain features  
177 that have been frequently used by scientists and exploited by the PMP (e.g., regridding, utilization of spatial/temporal  
178 bounds for computational operations) which motivated the development of the xCDAT. Completing the transition  
179 from CDAT to xCDAT is a technical priority for the next version of PMP.

180 To help advance open and reproducible science, the PMP has been maintained with an open-source policy  
181 with accompanying metadata for data reproducibility and reusability. The PMP code is distributed and released with  
182 version control. The installation process of PMP is streamlined and user-friendly, leveraging the *Anaconda* distribution  
183 and the *conda-forge* channel. By employing *conda* and *conda-forge*, users benefit from a simplified and efficient  
184 installation experience, ensuring seamless integration of PMP's functionality with minimal dependencies. This  
185 approach not only facilitates a straightforward deployment of the package but also enhances reproducibility and  
186 compatibility across different computing environments, thereby facilitating the accessibility and widespread adoption  
187 of PMP within the scientific community. The pointer to the installation instructions can be found in the Code and Data  
188 Availability section. The PMP's online documentation ([http://pcmdi.github.io/pcmdi\\_metrics/](http://pcmdi.github.io/pcmdi_metrics/)) also includes  
189 installation instructions and user demo Jupyter Notebooks. A database of pre-calculated PMP statistics for all AMIP  
190 and Historical simulations in the CMIP archive are also available online. The archive of these statistics, stored as  
191 JSON files (Crockford, 2006; Crockford and Morningstar, 2017), includes versioning details for all codes, and  
192 dependencies and data that were used for the calculations. These files provide the baseline results of the PMP (see the  
193 Code and Data Availability section for details). Advancements in model evaluation along with the number of models  
194 and complexity of simulations motivate more systematic documentation of performance summaries. With PMP  
195 workflow provenance information being recorded and the model and observational data standards maintained by  
196 PCMDI and colleagues, PMP strives to make all its results reproducible.

197

### 198 **3 Current PMP capabilities**

199 The capabilities of the PMP have been expanded beyond its traditional large-scale performance summaries  
200 of the mean climate (Gleckler et al., 2008; Taylor, 2001). Various evaluation metrics have been implemented to the  
201 PMP for climate variability such as El Niño-Southern Oscillation (ENSO) (Planton et al., 2021; Lee et al., 2021a),  
202 extratropical modes of variability (Lee et al., 2019, 2021b), intra-seasonal oscillation (Ahn et al., 2017), monsoons  
203 (Sperber and Annamalai, 2014), cloud feedback (Zelinka et al., 2022), and the characteristics of simulated  
204 precipitation (Pendergrass et al., 2020; Ahn et al., 2022, 2023) and extremes (Wehner et al., 2020, 2021). These PMP  
205 capabilities were built upon model performance tests that have resulted from research by PCMDI scientists and their  
206 collaborators. This section will provide an overview of each category of the current PMP evaluation metrics with their  
207 usage demonstrations.

208

#### 209 **3.1 Climatology**

210 Mean state metrics quantify how well models simulate observed climatological fields at a large scale, gauged  
211 by a suite of well-established statistics such as RMSE, mean absolute error (MAE), and pattern correlation that have  
212 been used in climate research for decades. The focus is on the coupled “Historical” and atmospheric-only AMIP (Gates  
213 et al., 1999) simulations which are well-suited for comparison with observations. The PMP extracts seasonally and  
214 annually averaged fields of multiple variables from large-scale observationally based datasets and results from model  
215 simulations. Different obs4MIPs-compliant reference datasets are used depending on the variable examined. When  
216 multiple reference datasets are available, one of them is considered as a “default” (e.g., see Table 1) while others are  
217 identified as “alternatives”. The default datasets are typically state-of-the-art products, but in general, we lack  
218 definitive measures as to which is the most accurate, so the PMP metrics are routinely calculated with multiple  
219 products so that it can be determined what difference the selection of alternative observations makes to judgment made  
220 about model fidelity. The suite of mean climate metrics (all area weighted) includes spatial and spatiotemporal RMSE,  
221 centered spatial RMSE, spatial-mean bias, spatial standard deviation, spatial pattern correlation, and spatial and  
222 spatiotemporal MAE of the annual or seasonal climatological time-mean (Gleckler et al., 2008). Often, a space-time  
223 statistic is used that gauges both the consistency of the observed and simulated climatological pattern as well as its  
224 seasonal evolution (see Eq. 1 from Gleckler et al., 2008). By default, results are available for selected large-scale  
225 domains, including: “Global”, “Northern Hemisphere (NH) Extratropics” (30°N-90°N), “Tropics” (30°S-30°N), and  
226 “Southern Hemisphere (SH) Extratropics” (30°S-90°S). For each domain, results can also be computed for the land  
227 and ocean, land only, or ocean only. These commonly used domains highlight the application of the PMP mean climate  
228 statistics at large to global scales, but we note that PMP allows users to define their own domains of interest, including  
229 at regional scales. Detailed instructions can be found on the PMP’s online documentation  
230 ([http://pcmdi.github.io/pcmdi\\_metrics](http://pcmdi.github.io/pcmdi_metrics)).

231 Although the primary deliverable of the PMP is the metrics, the PMP results can be visualized in various  
232 ways. For individual fields, we often first plot Taylor Diagrams, a polar plot leveraging the relationship between the  
233 centered RMSE, the pattern correlation, and the observed and simulated standard deviation (Taylor, 2001). The Taylor  
234 Diagram has become a standard plot in the model evaluation workflow across modeling centers and research

235 communities (see Sect. 5). To interpret results across CMIP models for many variables, we routinely construct  
236 normalized Portrait Plots or Gleckler Plots (Gleckler et al., 2008) that provide a quick-look examination of the  
237 strengths and weaknesses of different models. For example, in Figure 1, the PMP results display quantitative  
238 information of simulated seasonal climatologies of various meteorological model variables via a normalized global  
239 spatial RMSE (Gleckler et al., 2008). Variants of this plot have been widely used for presenting model evaluation  
240 results, for example, in the IPCC Fifth (Flato et al., 2014, Figures 9.7, 9.12, and 9.37) and Sixth Assessment Reports  
241 (Eyring et al., 2021, Chapter 3, Figure 3.42). Because the error distribution across models is variable dependent, the  
242 statistics are often normalized to help reveal differences, in this case via the median RMSE across all models (see  
243 Gleckler et al. 2008 for more details). This normalization enables a common color scale to be used for all statistics on  
244 the Portrait Plot, highlighting the relative strengths and weaknesses of different models. In this example (Fig. 1), an  
245 error of -0.5 indicates that a model's error is 50% smaller than the typical (median) error across all models, whereas  
246 an error of 0.5 is 50% larger than the typical error in the multi-model ensemble. In many cases, the horizontal bands  
247 in the Gleckler plots show that simulations from a given modeling center have similar error structures relative to the  
248 multi-model ensemble.

249 The Parallel Coordinate Plot (Inselberg, 1997, 2008, 2016; Johansson and Forsell, 2016) that retains the  
250 absolute value of the error statistics is used to complement the Portrait plot. Some previous studies have utilized  
251 Parallel Coordinate Plots for analyzing climate model simulations (e.g., Steed et al., 2012; Wong et al., 2014; Wang  
252 et al., 2017), but to date, only a few studies have applied it to collective multi-ESM evaluations (e.g., see Fig. 7 of  
253 Boucher et al., 2020). In the PMP, we generally construct Parallel Coordinate Plots using the same data as in a portrait  
254 plot. However, a fundamental difference is that metrics values can be more easily scaled to highlight absolute values  
255 rather than the normalized relative results of the portrait plot. In this way, the Portrait and Parallel Coordinate plots  
256 complement one another, and in some applications, it can be instructive to display both. Figure 2 shows the  
257 spatiotemporal RMSE, defined as the temporal average of spatial RMSE calculated in each month of the annual cycle,  
258 of CMIP5 and CMIP6 models in the format of Parallel Coordinate Plot. Each vertical axis represents a different scalar  
259 measure gauging a distinct aspect of model fidelity. While polylines are frequently used to connect data points from  
260 the same source (i.e., metric values from the same model, in our case) in Parallel Coordinate Plots, we display results  
261 from each model using an identification symbol to reduce visual clutter on the plot and help identify outlier models.  
262 In the example of Fig. 2, each vertical axis is aligned with the median value midway through its max/min range scale.  
263 Thus, for each axis, the models in the lower half of the plot perform better than the CMIP5-CMIP6 multi-model  
264 median, while in the upper half, the opposite is true. For each vertical axis that is for a different model variable, we  
265 have added violin plots (Hintze and Nelson, 1998) to show probability density functions representing the distributions  
266 of model performance obtained from CMIP5 (shaded in blue, left side of the axis) and CMIP6 (shaded in orange, right  
267 side of the axis). Medians of each CMIP5 and CMIP6 group are highlighted using polylines, which indicates that the  
268 RMSE is reduced in CMIP6 relative to CMIP5 in general for the majority of the subset of model variables.

269



## 270 3.2 *El Niño-Southern Oscillation*

271 The El Niño-Southern Oscillation (ENSO) is Earth’s dominant interannual mode of climate variability, which  
272 impacts global climate via both regional oceanic effects and far-reaching atmospheric teleconnections (McPhaden et  
273 al., 2006, 2020). In response to increasing interest in a community approach to ENSO evaluation in models (Bellenger  
274 et al., 2014), the International Climate and Ocean Variability, Predictability and Change (CLIVAR) Research Focus  
275 on ENSO in a Changing Climate, together with the CLIVAR Pacific Region Panel, developed the CLIVAR ENSO  
276 Metrics Package (Planton et al., 2021) which is now utilized within the PMP. The ENSO metrics used to  
277 assess/evaluate the models are grouped into three categories: *Performance* (i.e., background climatology and basic  
278 ENSO characteristics), *Teleconnections* (ENSO's worldwide teleconnections), and *Processes* (ENSO's internal  
279 processes and feedback). Planton et al. (2021) found that CMIP6 models generally outperform CMIP5 models in  
280 several ENSO metrics in particular for those related to tropical Pacific seasonal cycles and ENSO teleconnections.  
281 This effort is discussed in more detail in Planton et al. (2021), and detailed descriptions of each metric in the package  
282 are available in the ENSO Package online open-source code repository on its GitHub Wiki pages (see  
283 [https://github.com/CLIVAR-PRP/ENSO\\_metrics/wiki](https://github.com/CLIVAR-PRP/ENSO_metrics/wiki)).

284 Figure 3 demonstrates the application of the ENSO metrics to CMIP6, showing the magnitudes of inter-  
285 model and inter-ensemble spreads, along with observational uncertainty varying across metrics. For a majority of the  
286 ENSO Performance metrics model error and inter-model spread are substantially larger than observational uncertainty  
287 (Figs. 3a-n). This highlights the systematic biases like the double intertropical convergence zone (ITCZ) (Fig. 3a) that  
288 are persisting through CMIP phases (Tian and Dong, 2020). Similarly, ENSO Processes metrics (Figs. 3t-w) indicate  
289 large errors in the feedback loops generating SST anomalies, indicating a different balance of processes in the model  
290 and in the reference and possibly compensating errors (Bayr et al., 2019, Guilyardi et al. 2020). In contrast, for ENSO  
291 Teleconnection metrics, the observational uncertainty is substantially larger, thus challenging validation of model  
292 error (Figs. 3o-r). For some metrics, such as the ENSO duration (Fig. 3f), the ENSO Asymmetry metric (Fig. 3i), and  
293 the Ocean driven SST metric (Fig. 3s), there are larger inter-ensemble spreads than the inter-model spreads. From  
294 such results, Lee et al. (2021a) examined the inter-model and inter-member spread of these metrics from the large  
295 ensembles available from CMIP6 and the US CLIVAR Large Ensemble Working Group. They argued that to robustly  
296 characterize baseline ENSO characteristics and physical processes, larger ensemble sizes are needed, compared to  
297 existing state-of-the-art ensemble projects. By applying the ENSO metrics to historical and piControl simulations of  
298 CMIP6 via the PMP, Planton et al. (2023) developed equations based on statistical theory to estimate the required  
299 ensemble size for a user-defined uncertainty range.

300

## 301 3.3 *Extratropical Modes of Variability*

302 The PMP includes objective measures of the pattern and amplitude of extratropical modes of variability from  
303 PCMDI’s research, which has expanded beyond its traditional large-scale performance summaries to include  
304 interannual variability, considering increasing interest in setting an objective approach for the collective evaluation of  
305 multiple modes. Extratropical modes of variability (ETMoV) metrics in the PMP were developed by Lee et al. (2019a)  
306 that stem from earlier works (e.g., Stoner et al., 2009; Phillips et al., 2014). Lee et al. (2019a) illustrated a challenge

307 when evaluating modes of variability using the traditional empirical orthogonal functions (EOF). In particular, when  
308 a higher-order EOF of a model more closely corresponds to a lower-order observationally based EOF (or vice versa),  
309 it can significantly affect conclusions drawn about model performance. To circumvent this issue in evaluating the  
310 interannual variability modes, Lee et al. (2019a) used the Common Basis Function (CBF) approach that projects the  
311 observed EOF pattern onto model anomalies. This approach has been previously applied for the evaluation of  
312 intraseasonal variability modes (Sperber, 2004; Sperber et al., 2005). In the PMP, the CBF approach is taken as a  
313 default method, and the traditional EOF approach is also enabled as an option for the ETMoV metrics calculations.

314 The ETMoV metrics in the PMP measure simulated patterns and amplitudes of ETMoV, and quantify their  
315 agreement with observations (e.g., Lee et al., 2019a, 2021b). The PMP's ETMoV metrics evaluate 5 atmospheric  
316 modes – the Northern Annular Mode (NAM), North Atlantic Oscillation (NAO), Pacific North America pattern  
317 (PNA), North Pacific Oscillation (NPO), and Southern Annular Mode (SAM), and 3 ocean modes diagnosed by the  
318 variance of sea-surface temperature – Pacific Decadal Oscillation (PDO), North Pacific Gyre Oscillation (NPGO),  
319 and Atlantic Multi-decadal Oscillation (AMO). The AMO is included for experimental purposes, considering the  
320 significant uncertainty in detecting the AMO (Deser and Philips 2021; Zhao et al., 2022). The amplitude metric,  
321 defined as the ratio of standard deviations of the model and observed principal components, has been used to examine  
322 the evolution of the performance of models across different CMIP generations (Fig. 4). Green shading predominates,  
323 indicating where the simulated amplitude of variability is similar to observations. In some cases, such as for SAM in  
324 September-October-November (SON), the models overestimate the observed amplitude.

325 The PMP's ETMoV metrics have been used in several model evaluation studies. For example, Orbe et al.  
326 (2020) analyzed models from U.S. climate modeling groups including the U.S. Department of Energy (DOE), National  
327 Aeronautics and Space Administration (NASA), National Center for Atmospheric Research (NCAR), and National  
328 Oceanic and Atmospheric Administration (NOAA), where they found that the improvement in the ETMoV  
329 performance is highly dependent on mode and season, when comparing across different generations of those models.  
330 Sung et al. (2021) examined the performance of models run at the Korea Meteorological Administration (K-ACE and  
331 UKESM1) in reproducing ETMoVs from their Historical simulations, and concluded that these models reasonably  
332 capture most ETMoVs. Lee et al. (2021b) collectively evaluated ~130 models from CMIP3, 5, and 6 archive databases  
333 using their ~850 Historical and ~300 AMIP simulations, where they found the spatial pattern skill improved in CMIP6  
334 compared to CMIP5 or CMIP3 for most modes and seasons, while the improvement in amplitude skill is not clear.  
335 Arcodia et al. (2023) used the PMP to derive PDO and AMO to investigate their role in decadal variability of  
336 subseasonal predictability of precipitation over the western coast of North America and concluded that no significant  
337 relationship was found.

338

### 339 ***3.4 Intraseasonal Oscillation***

340 The PMP has implemented metrics for the Madden-Julian Oscillation (MJO; Madden and Julian, 1971, 1972,  
341 1994). The MJO is the dominant mode of tropical intraseasonal variability, characterized by a pronounced eastward  
342 propagation of large-scale atmospheric circulation coupled with convection with a typical periodicity of 30-60 days.

343 Selected metrics from the MJO diagnostics package, developed by the CLIVAR MJO Working Group (Waliser et al.,  
344 2009), have been implemented in the PMP following Ahn et al. (2017).

345 We have particularly focused on metrics for the MJO propagation: East/West power Ratio (EWR) and East  
346 power normalized by Observation (EOR). The EWR is proposed by Zhang and Hendon (1997) which is defined as  
347 the ratio of the total spectral power over the MJO band (eastward propagating, wavenumber 1-3 and period of 30-60  
348 days) to that of its westward propagating counterpart in the wavenumber-frequency power spectra. The EWR metric  
349 has been widely used in the community, to examine the robustness of the eastward propagating feature of the MJO  
350 (e.g., Hendon et al., 1999; Lin et al., 2006; Kim et al., 2009; Ahn et al., 2017). The EOR is formulated by normalizing  
351 a model's spectral power within the MJO band by the corresponding observed value. Ahn et al. (2017) showed EWRs  
352 and EORs of the CMIP5 models. Using daily precipitation, the PMP calculates EWR and EOR separately for boreal  
353 winter (November to April) and boreal summer (March to October). We apply the frequency-wavenumber  
354 decomposition method to precipitation from observations (GPCP-based; 1997-2010) and the CMIP5 and CMIP6  
355 Historical simulations for 1985-2004. For disturbances with wavenumbers 1-3 and frequencies corresponding to 30-  
356 60 days, it is clear in observations that the eastward propagating signal dominates over its westward propagating  
357 counterpart with an EWR value of about 2.49 (Fig. 5a). Figure 5b shows the wavenumber-frequency power spectrum  
358 from CMIP5 IPSL-CM5B-LR as an example, which has an EWR value that is comparable to the observed value.

359 Figure 6 shows the EWR from individual models' multiple ensemble members and their average. The average  
360 EWR of the CMIP6 model simulations is more realistic than that of the CMIP5 models. Interestingly, a substantial  
361 spread exists across models and also among ensemble members of a single model. For example, while the average  
362 EWR value for the CESM2 ensemble is 2.47 (close to 2.49 from the GPCP observations), the EWR values of the  
363 individual ensemble members range from 1.87 to 3.23. Kang et al. (2020) suggested that the ensemble spread in the  
364 propagation characteristics of the MJO can be attributed to the differences in the moisture mean state, especially its  
365 meridional moisture gradient. A cautionary note should be given to the fact that the MJO frequency and wavenumber  
366 windows are chosen to capture the spectral peak in observations. Thus, while the EWR provides an initial evaluation  
367 of the propagation characteristics of the observed and simulated MJO, it is instructive to look at the frequency-  
368 wavenumber spectra, as in some cases the dominant periodicity and wavenumber in a model may be different than in  
369 observations. It is worthwhile to note that the PMP can be used to obtain EWR and EOR of other daily variables for  
370 MJO analysis, such as outgoing longwave radiation (OLR) or zonal wind at 850 hPa (U-850) or 250 hPa (U-250), as  
371 shown in Ahn et al. (2017).

372

### 373 **3.5 Monsoons**

374 Based on the work of Sperber and Annamalai (2014), skill metrics in the PMP quantify how well models  
375 represent the onset, decay, and duration of regional monsoons. From observations and Historical simulations, the  
376 climatological pentad data of precipitation are area-averaged for six monsoon domains: All-India Rainfall, Sahel, Gulf  
377 of Guinea, North American Monsoon, South American Monsoon, and Northern Australia (Fig. 7). For the domains in  
378 the Northern Hemisphere, the 73 climatological pentads run from January to December, while for the domains in the  
379 Southern Hemisphere, the pentads run from July to June. For each domain, the precipitation is accumulated at each

380 subsequent pentad and then divided by the total precipitation to give the fractional accumulation of precipitation as a  
381 function of pentad. Thus, the annual cycle behavior is evaluated irrespective of whether a model has a dry or wet bias.  
382 Except for the Gulf of Guinea, the onset and decay of monsoon occur for a fractional accumulation of 0.2 and 0.8,  
383 respectively. Between these fractional accumulations, the accumulation of precipitation is nearly linear as the monsoon  
384 season progresses. Comparison of the simulated and observed onset, duration, and decay are presented in terms of the  
385 difference in the pentad index obtained from the model and observations (i.e., model minus observations). Therefore,  
386 negative values indicate that the onset or decay in the model occurs earlier than in observations, while positive values  
387 indicate the opposite. For duration, negative values indicate that for the model it takes fewer pentads to progress from  
388 onset to decay compared to observations (i.e., the simulated monsoon period is too short), while positive values  
389 indicate the opposite.

390 For CMIP5, we find systematic errors in the phase of the annual cycle of rainfall. The models are delayed in  
391 the onset of summer rainfall over India, the Gulf of Guinea, and the South American Monsoon, with early onset  
392 prevalent for the Sahel and the North American Monsoon. The lack of consistency in the phase error across all domains  
393 suggests that a “global” approach to the study of monsoons may not be sufficient to rectify the regional differences.  
394 Rather, regional process studies are necessary for diagnosing the underlying causes of the regionally specific  
395 systematic model biases over the different monsoon domains. Assessment of the monsoon fidelity in CMIP6 models  
396 using the PMP is in progress.

397

### 398 **3.6 Cloud feedback and mean-state**

399 Uncertainties in cloud feedback are the primary driver of model-to-model differences in climate sensitivity  
400 – the global temperature response to a doubling of atmospheric CO<sub>2</sub>. Recently, an expert synthesis of several lines of  
401 evidence spanning theory, high-resolution models, and observations was conducted to establish quantitative  
402 benchmark values (and uncertainty ranges) for several key cloud feedback mechanisms. The assessed feedbacks are  
403 those due to changes in high-cloud altitude, tropical marine low-cloud amount, tropical anvil cloud area, land cloud  
404 amount, middle latitude marine low-cloud amount, and high latitude low-cloud optical depth. The sum of these six  
405 components yields the total assessed cloud feedback, which is part of the overall radiative feedback that fed into the  
406 Bayesian calculation of climate sensitivity in Sherwood et al. (2020). Zelinka et al. (2022) estimated these same  
407 feedback components in climate models and evaluated them against the expert-judgment values determined in  
408 Sherwood et al. (2020), ultimately deriving a root mean square error metric that quantifies the overall match between  
409 each model’s cloud feedback and those determined through expert judgment.

410 Figure 8 shows the model-simulated values for each individual feedback computed in *amip-p4K* simulations  
411 as part of CMIP5 and CMIP6 alongside the expert judgment values. Each model is color-coded by its equilibrium  
412 climate sensitivity (determined using *abrupt-4xCO2* simulations as described in Zelinka et al., 2020), and the values  
413 from an illustrative model (GFDL-CM4) are highlighted. Among the key results apparent from this figure is that  
414 models typically underestimate the strength of both positive tropical marine low-cloud feedback and the negative anvil  
415 cloud feedback relative to the central expert assessed value. The sum of all six assessed feedback components is

416 positive in all but two models, with a multimodel mean value that is close to the expert-assessed value, but exhibits  
417 substantial intermodel spread.

418 In addition to evaluating the ability of models to match the assessed cloud feedback components, Zelinka et  
419 al. (2022) investigated whether models with less erroneous mean-state clouds tend to have smaller errors in their  
420 overall cloud feedback RMSE. This involved computing the mean-state cloud property error metric developed by  
421 Klein et al. (2013). This error metric quantifies the spatiotemporal error in climatological cloud properties for clouds  
422 with optical depths greater than 3.6, weighted by their net top-of-atmosphere (TOA) radiative impact. The  
423 observational baseline against which the models are compared comes from the International Satellite Cloud  
424 Climatology Project H-series Gridded Global (ISCCP HGG) dataset (Young et al., 2018). Zelinka et al. (2022) showed  
425 that models with smaller mean-state cloud errors tend to have stronger but not necessarily better (less erroneous) cloud  
426 feedback, which suggests that improving mean-state cloud properties does not guarantee improvement in the cloud  
427 response to warming. However, the models with the smallest errors in cloud feedback tend also to have less erroneous  
428 mean-state cloud properties, and no models with poor mean-state cloud properties have feedback in good agreement  
429 with expert judgment.

430 The PMP implementation of this code computes cloud feedback by differencing fields from *amip-p4K* and  
431 *amip* experiments and normalizing by the corresponding global mean surface temperature change rather than from  
432 differencing *abrupt-4xCO2* and *piControl* experiments and computing feedback via regression (as was done in Zelinka  
433 et al., 2022). This choice is made to reduce the computational burden and also because cloud feedbacks derived from  
434 these simpler atmosphere-only simulations have been shown to closely match those derived from fully coupled  
435 quadrupled CO<sub>2</sub> simulations (Qin et al., 2022). The code produces figures in which the user-specified model results  
436 are highlighted and placed in the context of the CMIP5 and CMIP6 multi-model results (e.g., Fig. 8).

### 437 438 **3.7 Precipitation**

439 Recognizing the importance of accurately simulating precipitation in ESMs and a lack of objective and  
440 systematic benchmarking for it, and motivated by discussions with WGNE and WGCM working groups of WCRP,  
441 the DOE has initiated an effort to establish a pathway to help modelers gauge improvement (U.S. DOE, 2020). The  
442 2019 DOE workshop “Benchmarking Simulated Precipitation in Earth System Models” generated two sets of  
443 precipitation metrics: *baseline* and *exploratory* metrics (Pendergrass et al., 2020). In the PMP, we have focused on  
444 implementing the *baseline* metrics for benchmarking simulated precipitation. In parallel, a set of *exploratory* metrics  
445 that could be added to metrics suites including PMP in the future was illustrated by Leung et al. (2022) to extend the  
446 evaluation scope to include process-oriented and phenomena-based diagnostics and metrics.

447 The *baseline* metrics gauge the consistency between ESMs and observations, focusing on the holistic set of  
448 observed rainfall characteristics (Fig. 9). For example, the spatial distribution of mean state precipitation and seasonal  
449 cycle are outcomes of the PMP’s Climatology metrics (described in Sect. 3.1), which provides collective evaluation  
450 statistics such as RMSE, standard deviation, and pattern correlation over various domains (e.g., global, NH and SH  
451 extratropics, and tropics, with each domain as a whole, and over land and ocean, in separate). Evaluation of  
452 precipitation variability across many timescales with PMP is documented in Ahn et al. (2022); we summarize some

453 of the findings here. The precipitation variability metric measures forced (diurnal and annual cycles) and internal  
454 variability across timescales (subdaily, synoptic, subseasonal, seasonal, and interannual) in a framework based on  
455 power spectra of 3-hourly total and anomaly precipitation. Overall, CMIP5 and CMIP6 models underestimate the  
456 internal variability, which is more pronounced in the higher frequency variability, while they overestimate the forced  
457 variability (Fig. 10). For the diurnal cycle, PMP includes metrics from Covey et al. (2016). Additionally, the intensity  
458 and distribution of precipitation are assessed following Ahn et al. (2023). Extreme daily precipitation indices and their  
459 20-year return values are calculated using a non-stationary Generalized Extreme Value statistical method. From the  
460 CMIP5 and CMIP6 historical simulations we evaluate model performance of these indices and their return values in  
461 comparison with gridded land-based daily observations. Using this approach, Wehner et al. (2020) found that at  
462 models' standard resolutions, no meaningful differences were found between the two generations of CMIP models.  
463 Wehner et al. (2021) extended the evaluation of simulated extreme precipitation to seasonal 3-hourly precipitation  
464 extremes produced by available HighResMIP models and concluded that the improvement is minimal with the models'  
465 increased spatial resolutions. They also noted that the order of operations of regridding and calculating extremes  
466 affects the ability of models to reproduce observations. Drought metrics developed by Xue and Ullrich (2021) are not  
467 implemented in PMP directly, but are wrapped by the Coordinated Model Evaluation Capabilities (CMEC; Ordonez  
468 et al. 2021), which is a parallel framework for supporting community-developed evaluation packages. Together, these  
469 metrics provide a streamlined workflow for running the entire baseline metrics via the PMP and CMEC that is ready  
470 for use by operational centers and in the CMIP7.

471

### 472 *3.8 Relating metrics to underlying diagnostics*

473 Considering the extensive collection of information generated from the PMP, efforts have supported  
474 improved visualizations of metrics using interactive graphic user interfaces. These capabilities can facilitate the  
475 interpretation and synthesis of vast amounts of information associated with the diverse metrics and the underlying  
476 diagnostics from which they were derived. Via the interactive navigation interface, we can explore the underlying  
477 diagnostics behind the PMP's summary plots. On the PCMDI website, we provide interactive graphical interfaces to  
478 enable navigating the supporting plots to the underlying diagnostics of each model's ensemble members and their  
479 average. For example, on the interactive mean climate plots ([https://pcmdi.llnl.gov/metrics/mean\\_clim/](https://pcmdi.llnl.gov/metrics/mean_clim/)), hovering the  
480 mouse cursor over a square or triangle in the Portrait Plot, or over the markers or lines in the Parallel Coordinate Plot,  
481 reveals the diagnostic plot from which the metrics were generated. It allows the user to toggle between several metrics  
482 (e.g., RMSE, bias, and correlation) and regions (e.g., global, Northern/Southern Hemisphere, and Tropics), along with  
483 relevant provenance information. Users can click on the interactive plots to get dive-down diagnostics information for  
484 the model of interest which provides detailed analysis to better understand how the metric was calculated. As with the  
485 PMP's mean climate metrics output, we currently provide interactive summary graphics for ENSO  
486 (<https://pcmdi.llnl.gov/metrics/enso/>), extratropical modes of variability  
487 ([https://pcmdi.llnl.gov/metrics/variability\\_modes/](https://pcmdi.llnl.gov/metrics/variability_modes/)), monsoon (<https://pcmdi.llnl.gov/metrics/monsoon/>), MJO  
488 (<https://pcmdi.llnl.gov/metrics/mjo/>), and precipitation benchmarking (<https://pcmdi.llnl.gov/metrics/precip/>). We  
489 plan to expand this capability to other metrics in the PMP, such as the cloud feedback analysis. The majority of the

490 PMP’s interactive plots have been developed using Bokeh (<https://bokeh.org/>), a Python data visualization library that  
491 enables the creation of interactive plots and applications for web browsers.

492

#### 493 **4 Model Benchmarking**

494 While the PMP originally focused on evaluating multiple models (e.g., Gleckler et al., 2008), in parallel there  
495 has been increasing interest from model developers and modeling centers to leverage the PMP to track performance  
496 evolution in the model development cycle, as discussed in Gleckler et al. (2016). For example, metrics from the PMP  
497 have been used to document performance of ESMs developed in the U.S. DOE Exascale Earth System Model (E3SM;  
498 Caldwell et al., 2019; Golaz et al., 2019; Rasch et al., 2019; Hannah et al., 2021; Tang et al., 2021), NOAA  
499 Geophysical Fluid Dynamics Laboratory (GFDL; Zhao et al., 2018), Institut Pierre-Simon Laplace (IPSL; Boucher et  
500 al., 2020; Planton et al., 2021), National Institute of Meteorological Sciences-Korea Meteorological Administration  
501 (NIMS-KMA; Sung et al., 2021), University of California, Los Angeles (Lee et al., 2019b), and the Community  
502 Integrated Earth System Model (CIESM) project (Lin et al., 2020).

503 To make the PMP more accessible and useful for modeling groups, efforts are underway to broaden workflow  
504 options. Currently, a typical application involves computing a particular class of performance metrics (e.g., mean  
505 climate) for all CMIP simulations available via ESGF. To facilitate the ability of modeling groups to routinely use the  
506 PMP during their development process, we are working to provide a customized workflow option to run all the PMP  
507 metrics more seamlessly on a single model, and to compare these results with a database of PMP results obtained from  
508 CMIP simulations (see Code and Data Availability section). Via the PMP-documented and pre-calculated metrics  
509 from simulations in the CMIP archive, it is possible to readily incorporate CMIP results into the assessment of new  
510 simulations, without retrieving all CMIP simulations and recomputing the results. The resulting quick-look feedback  
511 can highlight model improvement (or deterioration) and can assist in determining development priorities or in the  
512 selection of a new model version.

513 As an example, here, we show PMP results obtained from GFDL-CM3 from CMIP5 and GFDL-CM4 from  
514 CMIP6, for a demonstration of using the Taylor Diagram to compare versions of a given model (Fig. 11). One  
515 advantage of the Taylor Diagram is that it collectively represents three statistics (i.e., centered RMSE, standard  
516 deviation, and correlation) in a single plot (Taylor, 2001), which synthesizes the performance intercomparison of  
517 multiple models (or different versions of a model). In this example, four variables were selected to summarize  
518 performance evolution (shown by arrows) in multiple seasons. Except for boreal winter, both model versions are  
519 nearly identical in terms of net TOA radiation, however in all seasons the longwave cloud radiative effect is clearly  
520 improved in the newer model version. The TOA flux improvements likely contributed to the precipitation  
521 improvements, by improving the balances of radiative cooling and latent heating. The improvement in the newer  
522 model version is consistent with that documented by Held et al., (2019) and evident via the arrow directions pointing  
523 to the observational reference point.

524 Parallel Coordinate Plots can also be used to summarize the comparison of two simulations for their  
525 performance. In Fig 12, we demonstrate the comparison of selected metrics: the mean climate (see Sect. 3.1), ENSO  
526 (Sect. 3.2), and ETMoV (Sect. 3.3). To facilitate comparison of a subset of models, a few models can be selected and

527 highlighted as connected lines across individual vertical axes on the plot. A proposed application of it from PMP is to  
528 select two models or two versions of a model to contrast their performance (solid lines) against the backdrop of results  
529 from other models, shown as violin plots for the distribution of statistics from other models on each vertical axis. In  
530 this example, we contrast the performance of two GFDL models: GFDL-CM3 and GFDL-CM4. Fig 12a is a modified  
531 version of Figure 2 that is designed to highlight the difference in performance more efficiently. Each vertical axis  
532 indicates performance for each metric defined for climatology of variables (i.e., temporally averaged spatial RMSE  
533 of annual cycle climatology patterns, Fig. 12a), ENSO characteristics (Fig. 12b), or interannual variability mode  
534 obtained from seasonal or monthly averaged time series (Fig. 12c). It is shown that GFDL-CM4 is superior to GFDL-  
535 CM3 for most cases across selected metrics (downward arrows in green) while inferior for a few cases (upward arrows  
536 in red), which is consistent with previous findings (Held et al., 2019; Planton et al., 2021; Chen et al., 2021). Such  
537 applications of the Parallel Coordinate Plot can enable quick overall assessment and tracking of the ESM performance  
538 evolution during its development cycle. More examples showing other models are available in the Supplementary  
539 material (Figs. S1 to S3).

540 It is worth noting that there have been efforts to coalesce objective model evaluation concepts used in the  
541 research community (e.g., Knutti et al., 2010). However, the field continues to evolve rapidly with definitions still  
542 being debated and finessed. Via the PMP, we produce hundreds of summary statistics, enabling a broad net to be cast  
543 in the objective characterization of a simulation, at times helping modelers identify previously unknown deficiencies.  
544 For benchmarking, efforts are underway to establish a more targeted path which likely involves a consolidated set of  
545 carefully selected metrics.

546

## 547 **5 Discussion**

548 Efforts are underway to include new metrics into the PMP to advance the systematic objective evaluation of  
549 ESMs. For example, in coordination with the World Meteorological Organization (WMO)'s WGNE MJO Task Force,  
550 additional candidate MJO metrics for PMP inclusion have been identified to facilitate more comprehensive  
551 assessments of the MJO. Implementation of metrics for MJO amplitude, periodicity, and structure into the PMP is  
552 planned. An ongoing collaboration with NCAR aims to incorporate metrics related to the upper atmosphere,  
553 specifically the Quasi-Biennial Oscillation (QBO) and QBO-MJO metrics (e.g. Kim et al., 2020). We also have plans  
554 to grow the scope of PMP beyond its traditional atmospheric realm, for example including the ocean and polar regions  
555 through collaboration with the U.S. DOE's project entitled High Latitude Application and Testing of ESMs (HiLAT,  
556 <https://www.hilat.org/>). In addition, the PMP framework is also well poised to contribute to high-resolution climate  
557 modeling activities, such as the High-Resolution Model Intercomparison Project (HighResMIP; Haarsma et al., 2016)  
558 and the DYnamics of the Atmospheric general circulation Modeled On Non-hydrostatic Domains (DYAMOND;  
559 Stevens et al., 2019). This motivates the development of specialized metrics for high-resolution models, targeting the  
560 simulation features enabled by high-resolution models. Another potential avenue for the PMP involves leveraging  
561 Machine Learning (ML) techniques, and other state-of-the-art data science techniques being used for process-oriented  
562 ESM evaluation works (e.g., Nowack et al., 2020; Labe and Barnes, 2022; Dalelane et al., 2023). Applications of ML  
563 detection, such as for storms using TempestExtremes (Ullrich and Zarzycki 2017; Ullrich et al., 2021) and fronts (e.g,



564 Biard and Kunkel, 2019), can enable additional specialized storm metrics for high-resolution simulations. For  
565 convection-permitting models, yet more storm metrics can be applied such as Mesoscale convective systems.  
566 Atmospheric blocking metrics and atmospheric river evaluation metrics using the ML pattern detection capabilities in  
567 the latest TempestExtremes (Ullrich et al., 2021) are currently under development to be implemented into the PMP.  
568 These example enhancements of the PMP are indicative of an increasing priority to target regional simulation  
569 characteristics. With a deliberate emphasis on processes intrinsic to specific regions, this may lead to enabling  
570 potential applications of the PMP within the regional climate modeling activities such as the Coordinated Regional  
571 Downscaling Experiment (CORDEX; Gutowski Jr. et al., 2016).

572 The comprehensive database of PMP results offers a resource for exploring the range of structural errors in  
573 CMIP class models and their interrelationships. For example, examination of cross-metric relationships between  
574 mean-state and variability biases can shed additional light on the propagation of errors (e.g., Kang et al., 2020; Lee et  
575 al., 2021b). There continues to be interest in ranking models for specific applications (e.g., Ashfaq et al., 2022;  
576 Goldenson et al., 2023; Longmate et al., 2023; Papalexou et al., 2020; Singh and AchutaRao, 2020) or to “move  
577 beyond one model one vote” in multi-model analysis to reduce uncertainties in the spread of multi-model projections  
578 (e.g., Knutti, 2010; Knutti et al., 2017; Sanderson et al., 2017; Herger et al., 2018; Hausfather et al., 2022; Merrifield  
579 et al., 2023). While we acknowledge potential interests in using the results of the PMP or equivalent to rank models  
580 or identify performance outliers (e.g., Sanderson and Wehner, 2017), we believe the many challenges associated with  
581 model weighting are application dependent, and thus leave it up to users of the PMP to make those judgments.

582 In addition to the scientific challenges associated with diversifying objective summaries of model  
583 performance, there is potential to leverage rapidly evolving technologies, including new open-source tools and  
584 methods available to scientists. We expect that the ongoing PMP code modernization effort to fully adapt the xCDAT  
585 and xarray will facilitate greater community involvement. As the PMP evolves with these technologies we will  
586 continue to maintain rigor in the calculation of statistics for the PMP metrics, for example by incorporating the latest  
587 advancements in the field. A prominent example in the objective comparison of models and observations involves the  
588 methodology of horizontal interpolation, and in future versions of the PMP we are planning a more stringent  
589 conservation method (Taylor, 2024). To improve the clarity of key messages from multivariate PMP metrics data, we  
590 will consider implementing the advances in high-dimensional data visualization, e.g., the circular plot discussed in  
591 Lee et al. (2018b) and variations of Parallel Coordinate Plots proposed in this paper and by Hassan et al. (2019) and  
592 Lu et al. (2020).

593 Current progress towards systematic model evaluation is exemplified by the diversity of tools being  
594 developed (e.g., the PMP, ESMValTool, MDTF, ILAMB, IOMB, and other packages). Each of these tools has its own  
595 scientific priorities and technical approaches. We believe that this diversity has made, and will continue to make, the  
596 model evaluation process even more comprehensive and successful. The fact that there is some overlap in a few cases  
597 is advantageous because it enables the cross-verification of results, which is particularly useful in more complex  
598 analyses. Despite possible advantages, having no single best or widely accepted approach for the community to follow,  
599 does introduce complexity to the coordination of model evaluation. To facilitate the collective usage of individual  
600 evaluation tools, the CMEC has initiated the development of a unified code base that technically coordinates the

601 operation of distinct but complementary tools (Ordóñez et al. 2021). Currently, the PMP, ILAMB, MDTF, and ASoP  
602 have become CMEC-compliant by adopting common interface standards that define how evaluation tools interact  
603 with observational data and climate model output. We expect that CMEC can also help the model evaluation  
604 community to establish standards for archiving the metrics output, much as the community did for the conventions to  
605 describe climate model data (e.g., CMIP application of CF Metadata Conventions (<http://cfconventions.org/>); Hassell  
606 et al., 2017; Eaton et al., 2022).

607

## 608 **6 Summary and Conclusion**

609 The PCMDI has actively developed the PMP with support from the U.S. DOE to improve the understanding  
610 of ESMs and to provide systematic and objective ESM evaluation capabilities. With its focus on physical climate, the  
611 current evaluation categories enabled in the PMP include seasonal and annual climatology of multiple variables,  
612 ENSO, various variability modes in the climate system, MJO, monsoon, cloud feedback and mean state, and simulated  
613 precipitation characteristics. The PMP provides quasi-operational ESM evaluation capabilities that can be rapidly  
614 deployed to objectively summarize a diverse suite of model behavior with results made publicly available. This can  
615 be of value in the assessment of community intercomparisons like CMIP, the evaluation of large ensembles, or the  
616 model development process. By documenting objective performance summaries produced by the PMP and making  
617 them available via detailed version control, additional research is made possible beyond the baseline model evaluation,  
618 model intercomparison, and benchmarking. The outcomes of PMP's calculations applied to the CMIP archive  
619 culminate in the PCMDI Simulation Summary (<https://pcmdi.llnl.gov/metrics/>) that has served as a comprehensive  
620 data portal for objective model-to-observation comparisons and model-to-model benchmarking and intercomparisons.  
621 Special attention is dedicated to the most recent ensemble of models contributing to CMIP6. By offering a diverse and  
622 comprehensive suite of evaluation capabilities, the PMP framework equips model developers with quantifiable  
623 benchmarks to validate and enhance model performance.

624 We expect that the PMP will continue to play a crucial role in benchmarking ESMs. Improvements in the  
625 PMP, along with progress in interconnected MIP community projects, will greatly contribute to advancing the  
626 evaluation of ESMs including in connection to the community efforts (e.g., the CMIP Benchmarking Task Team).  
627 Enhancements in version control and transparency within obs4MIPs are set to enhance the provenance and  
628 reproducibility of PMP results, thereby strengthening the foundation for rigorous and repeatable performance  
629 benchmarking. The PMP's collaboration with the CMIP Forcing Task Team, through the Input4MIPs (Durack et al.,  
630 2018) and the CMIP6Plus projects, will further expand the utility of performance metrics in identifying problems  
631 associated with the forcing dataset and their application and use in reproducing the observed record of historical  
632 climate. Furthermore, as ESMs advance towards more operationalized configurations to meet the demands of decision-  
633 making processes (Jakob et al., 2023), the PMP holds significant potential to provide interoperable ESM evaluation  
634 and benchmarking capabilities to the community.

635 **Appendix A: Table of acronyms**

636

<b>Acronym</b>	<b>Description</b>
AMIP	Atmospheric Model Intercomparison Project
AMO	Atlantic Multi-decadal Oscillation
ARM	Atmospheric Radiation Measurement
ASoP	Analyzing Scales of Precipitation
CBF	Common Basis Function
CDAT	Community Data Analysis Tools
CIESM	Community Integrated Earth System Model
CLIVAR	Climate and Ocean Variability, Predictability and Change
CMEC	Coordinated Model Evaluation Capabilities
CMIP	Coupled Model Intercomparison Project
CMOR	Climate Model Output Rewriter
CVDP	Climate Variability Diagnostics Package
DOE	U.S. Department of Energy
ENSO	El Niño-Southern Oscillation
EOF	Empirical Orthogonal Functions
EOR	East power normalized by Observation

ESGF	Earth System Grid Federation
ESM	Earth System Model
ESMAC Diags	Earth System Model Aerosol–Cloud Diagnostics
ETMoV	Extratropical modes of variability
EWR	East/West power Ratio
GFDL	Geophysical Fluid Dynamics Laboratory
ILAMB	International Land Model Benchmarking
IOMB	International Ocean Model Benchmarking
IPCC	Intergovernmental Panel on Climate Change
IPSL	Institut Pierre-Simon Laplace
ISCCP HGG	International Satellite Cloud Climatology Project H-series Gridded Global
ITCZ	Intertropical Convergence Zone
JSON	JavaScript Object Notation
MAE	Mean Absolute Error
MDTF	Model Diagnostics Task Force
MIPs	Model Intercomparison Projects
MJO	Madden-Julian Oscillation
NAM	Northern Annular Mode

NAO	North Atlantic Oscillation
NASA	National Aeronautics and Space Administration
NCAR	National Center for Atmospheric Research
NetCDF	Network Common Data Form
NH	Northern Hemisphere
NIMS-KMA	National Institute of Meteorological Sciences-Korea Meteorological Administration
NOAA	National Oceanic and Atmospheric Administration
NPGO	North Pacific Gyre Oscillation
NPO	North Pacific Oscillation
PCMDI	Program for Climate Model Diagnosis and Intercomparison
PDO	Pacific Decadal Oscillation
PMP	PCMDI Metrics Package
PNA	Pacific North America pattern
RCMES	Regional Climate Model Evaluation System
RMSE	Root-Mean-Square Error
SAM	Southern Annular Mode
SH	Southern Hemisphere
SST	Sea Surface Temperature

TOA Top of Atmosphere

WCRP World Climate Research Programme

WGCM Working Group on Coupled Models

WGNE Working Group on Numerical Experimentation

xCDAT Xarray Climate Data Analysis Tools

638 **Code and Data Availability**

639 The source code of the PMP (Lee et al., 2023b) is available as an open-source Python package:  
640 [https://github.com/PCMDI/pcmdi\\_metrics](https://github.com/PCMDI/pcmdi_metrics) (last access: 4 April 2024) with all released versions archived on Zenodo  
641 DOI: <https://doi.org/10.5281/zenodo.592790> (last access: 4 April 2024). The online documentation is available at  
642 [http://pcmdi.github.io/pcmdi\\_metrics](http://pcmdi.github.io/pcmdi_metrics) (last access: 4 April 2024). The PMP results database (Lee et al., 2023a) that  
643 includes calculated metrics is available on the GitHub repository at  
644 [https://github.com/PCMDI/pcmdi\\_metrics\\_results\\_archive](https://github.com/PCMDI/pcmdi_metrics_results_archive) (last access: 4 April 2024) with versions archived on  
645 Zenodo DOI: <https://doi.org/10.5281/zenodo.10181201> (last access: 4 April 2024). PMP's installation process is  
646 streamlined using the *Anaconda* distribution and the *conda-forge* channel ([https://anaconda.org/conda-](https://anaconda.org/conda-forge/pcmdi_metrics)  
647 [forge/pcmdi\\_metrics](https://anaconda.org/conda-forge/pcmdi_metrics), last access: 4 April 2024). The installation instructions are available at  
648 [http://pcmdi.github.io/pcmdi\\_metrics/install.html](http://pcmdi.github.io/pcmdi_metrics/install.html) (last access: 4 April 2024). The interactive visualizations of the  
649 PMP results are available on the PCMDI website at <https://pcmdi.llnl.gov/metrics> (last access: 4 April 2024). The  
650 CMIP5 and CMIP6 model outputs and obs4MIPs datasets used in this paper are available via the Earth System Grid  
651 Federation at <https://esgf-node.llnl.gov/> (last access: 4 April 2024).

652

653 **Author Contributions**

654 All authors contributed to the design and implementation of the research, analysis of the results, and to writing of the  
655 manuscript. All authors contributed to the development of codes/metrics in the PMP, its ecosystem tools, and/or the  
656 establishment of use cases. JL and PJG led and coordinated the paper with input from all authors.

657

658 **Competing interests**

659 At least one of the coauthors is a member of the editorial board of *Geosic. Model Dev.*. The peer-review process was  
660 guided by an independent editor, and the authors also have no other competing interests to declare.

661

662 **Acknowledgment**

663 We acknowledge the World Climate Research Programme, which, through its Working Group on Coupled Modeling,  
664 coordinated and promoted CMIP6. We thank the climate modeling groups for producing and making available their  
665 model output, the Earth System Grid Federation (ESGF) for archiving the data and providing access, and the multiple  
666 funding agencies that support CMIP6 and ESGF. This work is performed under the auspices of the U.S. DOE by  
667 Lawrence Livermore National Laboratory (LLNL) under Contract No. DE-AC52-07NA27344. Efforts of JL, PJG,  
668 MA, AO, PU, KET, PD, CB, MDZ, LC, and BD were supported by the Regional and Global Model Analysis (RGMA)  
669 program of the U.S. Department of Energy (DOE) Office of Science (OS), Biological and Environmental Research  
670 (BER) program. MFW was supported by the Director, OS, BER of the U.S. DOE through the RGMA program under  
671 Contract No. DE340AC02-05CH11231. AGP was supported by U.S. DOE through BER RGMA through Award  
672 Number DE-SC0022070 and via National Science Foundation (NSF) IA 1947282, and by National Center for  
673 Atmospheric Research (NCAR), which is a major facility sponsored by the NSF under Cooperative Agreement No.  
674 1852977. YYP and EG were supported by the Agence Nationale de la Recherche ARISE project, under Grant ANR-

675 18-CE01-0012, and the Belmont project GOTHAM, under Grant ANR-15-JCLI-0004-01, the European  
676 Commission’s H2020 Programme “Infrastructure for the European Network for Earth System Modelling Phase 3 (IS-  
677 ENES3)” project under Grant Agreement 824084. DK was supported by the New Faculty Startup Fund from Seoul  
678 National University and the KMA R&D program (KMI2022-01313). The authors thank Program Manager Renu  
679 Joseph of the U.S. DOE for the support and advocacy for the Program for Climate Model Diagnosis and  
680 Intercomparison (PCMDI) project and the PMP. We thank Stephen Klein for his leadership for the PCMDI project  
681 from 2019 to 2022. We acknowledge contributions from our LLNL colleagues, Lina Muryanto and Zeshawn Shaheen  
682 (Now at Google LLC) during the early stage of the PMP, and Sasha Ames, Jeff Painter, Chris Mauzey, and Stephen  
683 Po-Chedley for the PCMDI’s CMIP database management. The authors also thank Liping Zhang for her comments  
684 during GFDL’s internal review process.

685

## 686 **References**

687 Adler, R.F., Sapiano, M. R., Huffman, G.J., Wang, J.J., Gu, G., Bolvin, D., Chiu, L., Schneider, U., Becker, A., Nelkin,  
688 E., Xie, P., Ferraro, R., Shin, D.-B.: The Global Precipitation Climatology Project (GPCP) monthly analysis  
689 (new version 2.3) and a review of 2017 global precipitation. *Atmosphere*, 9, 138,  
690 <https://doi.org/10.3390/atmos9040138>, 2018.

691 Ahn, M.-S., Kim, D. H., Sperber, K. R., Kang, I.-S., Maloney, E. D., Waliser, D. E., and Hendon, H. H.: MJO  
692 simulation in CMIP5 climate models: MJO skill metrics and process-oriented diagnosis, *Clim. Dynam.*, 49,  
693 4023–4045, <https://doi.org/10.1007/s00382-017-3558-4>, 2017.

694 Ahn, M.-S., Gleckler, P. J., Lee, J., Pendergrass, A. G., and Jakob, C.: Benchmarking Simulated Precipitation  
695 Variability Amplitude across Time Scales, *J. Climate*, 35, 3173–3196, <https://doi.org/10.1175/jcli-d-21-0542.1>, 2022.

697 Ahn, M.-S., Ullrich, P. A., Gleckler, P. J., Lee, J., Ordonez, A. C., and Pendergrass, A. G.: Evaluating precipitation  
698 distributions at regional scales: a benchmarking framework and application to CMIP5 and 6 models, *Geosci.  
699 Model Dev.*, 16, 3927–3951, <https://doi.org/10.5194/gmd-16-3927-2023>, 2023.

700 Arcodia, M., Barnes, E. A., Mayer, K., Lee, J., Ordonez, A., and Ahn, M.-S.: Assessing decadal variability of  
701 subseasonal forecasts of opportunity using explainable AI, *Environ. Res.*, 2, 045002,  
702 <https://doi.org/10.1088/2752-5295/aced60>, 2023.

703 Ashfaq, M., Rastogi, D., Kitson, J., Abid, M. A., and Kao, S.-C.: Evaluation of CMIP6 GCMs over the CONUS for  
704 downscaling studies, *J. Geophys. Res.-Atmos.*, 127, e2022JD036659.  
705 <https://doi.org/10.1029/2022JD036659>, 2022.

706 Bayr, T., Wengel, C., Latif, M., Dommenges, D., Lübbecke, J., and Park, W.: Error compensation of ENSO  
707 atmospheric feedbacks in climate models and its influence on simulated ENSO dynamics, *Clim. Dynam.*, 53,  
708 155–172, <https://doi.org/10.1007/s00382-018-4575-7>, 2019.

709 Biard, J. C. and Kunkel, K. E.: Automated detection of weather fronts using a deep learning neural network, *Adv.  
710 Stat. Clim. Meteorol. Oceanogr.*, 5, 147–160, <https://doi.org/10.5194/ascmo-5-147-2019>, 2019.



711 Bellenger, H., Guilyardi, E., Leloup, J., Lengaigne, M., and Vialard, J.: ENSO representation in climate models: from  
712 CMIP3 to CMIP5, *Clim. Dynam.*, 42, 1999–2018, <https://doi.org/10.1007/s00382-013-1783-z>, 2013.

713 Boucher, O., Servonnat, J., Albright, A. L., Aumont, O., Balkanski, Y., Bastrikov, V., Bekki, S., Bonnet, R., Bony,  
714 S., Bopp, L., Braconnot, P., Brockmann, P., Cadule, P., Caubel, A., Cheruy, F., Codron, F., Cozic, A., Cugnet,  
715 D., D’Andrea, F., Davini, P., De Lavergne, C., Denvil, S., Deshayes, J., Devilliers, M., Ducharne, A.,  
716 Dufresne, J. L., Dupont, E., Ethé, C., Fairhead, L., Falletti, L., Flavoni, S., Foujols, M. A., Gardoll, S.,  
717 Gastineau, G., Ghattas, J., Grandpeix, J. Y., Guenet, B., Lionel, E. G., Guilyardi, E., Guimberteau, M.,  
718 Hauglustaine, D., Hourdin, F., Idelkadi, A., Joussaume, S., Kageyama, M., Khodri, M., Krinner, G., Lebas,  
719 N., Levvasseur, G., Lévy, C., Li, L., Lott, F., Lurton, T., Luysaert, S., Madec, G., Madeleine, J.-B.,  
720 Maignan, F., Marchand, M., Marti, O., Mellul, L., Meurdesoif, Y., Mignot, J., Musat, I., Otlé, C., Peylin, P.,  
721 Planton, Y., Polcher, J., Rio, C., Rochetin, N., Rousset, C., Sepulchre, P., Sima, A., Swingedouw, D.,  
722 Thiéblemont, R., Traore, A. K., Vancoppenolle, M., Vial, J., Vialard, J., Viovy, N., and Vuichard, N.:  
723 Presentation and evaluation of the IPSL-CM6A-LR Climate Model, *J. Adv. Model. Earth Sy.*, 12,  
724 <https://doi.org/10.1029/2019ms002010>, 2020.

725 Caldwell, P., Mametjanov, A., Tang, Q., Van Roekel, L., Golaz, J.-C., Lin, W., Bader, D. C., Keen, N. D., Feng, Y.,  
726 Jacob, R., Maltrud, M., Roberts, A., Taylor, M. A., Veneziani, M., Wang, H., Wolfe, J. D., Balaguru, K.,  
727 Cameron-Smith, P. J., Dong, L., Klein, S. A., Leung, L. R., Li, H., Li, Q., Liu, X., Neale, R., Pinheiro, M.  
728 C., Qian, Y., Ullrich, P. A., Xie, S., Yang, Y., Zhang, Y., Zhang, K., and Zhou, T.: The DOE E3SM Coupled  
729 Model Version 1: description and results at high resolution, *J. Adv. Model. Earth Sy.*, 11, 4095–4146,  
730 <https://doi.org/10.1029/2019ms001870>, 2019.

731 Chen, H.-C., Jin, F.-F., Zhao, S., Wittenberg, A. T., and Xie, S.: ENSO dynamics in the E3SM-1-0, CESM2, and  
732 GFDL-CM4 climate models, *J. Climate*, 34, 9365–9384, <https://doi.org/10.1175/JCLI-D-21-0355.1>, 2021.

733 Collier, N., Hoffman, F. M., Lawrence, D. M., Keppel-Aleks, G., Koven, C. D., Riley, W. J., Mu, M., and Randerson,  
734 J. T.: The International Land Model Benchmarking (ILAMB) System: Design, theory, and implementation,  
735 *J. Adv. Model. Earth Sy.*, 10, 2731–2754, <https://doi.org/10.1029/2018ms001354>, 2018.

736 Covey, C., AchutaRao, K., Cubasch, U., Jones, P., Lambert, S. J., Mann, M., Phillips, T. J., and Taylor, K. E.: An  
737 overview of results from the Coupled Model Intercomparison Project, *Global. Planet. Change.*, 37, 103–133,  
738 [https://doi.org/10.1016/s0921-8181\(02\)00193-5](https://doi.org/10.1016/s0921-8181(02)00193-5), 2003.

739 Covey, C., Gleckler, P. J., Doutriaux, C., Williams, D. N., Dai, A., Fasullo, J. T., Trenberth, K. E., and Berg, A.:  
740 Metrics for the diurnal cycle of precipitation: toward routine benchmarks for climate models, *J. Climate*, 29,  
741 4461–4471, <https://doi.org/10.1175/jcli-d-15-0664.1>, 2016.

742 Crockford, D.: The application/json media type for javascript object notation (json) (No. rfc4627), [https://www.rfc-  
743 editor.org/rfc/pdf/rfc4627.txt.pdf](https://www.rfc-editor.org/rfc/pdf/rfc4627.txt.pdf) (last access: 4 April 2024), 2006.

744 Crockford, D. and Morningstar, C.: The JSON Data Interchange Syntax, ECMA-404, ECMA International, 2017.

745 Dalelane, C., Winderlich, K., and Walter, A.: Evaluation of global teleconnections in CMIP6 climate projections using  
746 complex networks, *Earth Syst. Dynam.*, 14, 17–37, <https://doi.org/10.5194/esd-14-17-2023>, 2023.

747 Dawson, A.: eofs: A Library for EOF Analysis of Meteorological, Oceanographic, and Climate Data, *J. Open Res.*  
748 *Software*, 4, e14, <https://doi.org/10.5334/jors.122>, 2016.

749 Dee, D. P., Uppala, S. M., Simmons, A. J., Berrisford, P., Poli, P., Kobayashi, S., Andrae, U., Balmaseda, M. A.,  
750 Balsamo, G., Bauer, P., Bechtold, P., Beljaars, A. C. M., van de Berg, L., Bidlot, J., Bormann, N., Delsol,  
751 C., Dragani, R., Fuentes, M., Geer, A. J., Haimberger, L., Healy, S. B., Hersbach, H., Hólm, E. V., Isaksen,  
752 L., Kållberg, P., Köhler, M., Matricardi, M., McNally, A. P., Monge-Sanz, B. M., Morcrette, J.-J., Park, B.-  
753 K., Peubey, C., de Rosnay, P., Tavolato, C., Thépaut, J.-N., and Vitart, F.: The ERA-Interim reanalysis:  
754 Configuration and performance of the data assimilation system, *Q. J. Roy. Meteor. Soc.*, 137, 553–597,  
755 <https://doi.org/10.1002/qj.828>, 2011

756 Deser, C. and Phillips, A. S.: Defining the internal component of Atlantic multidecadal variability in a changing  
757 climate, *Geophys. Res. Lett.*, 48, <https://doi.org/10.1029/2021gl095023>, 2021.

758 Doutriaux, C., Nadeau, D., Wittenburg, S., Lipsa, D., Muryanto, L., Chaudhary, A., and Williams, D. N.: CDAT/cdat:  
759 CDAT 8.1, Zenodo [Code], <https://doi.org/10.5281/zenodo.2586088>, 2019.

760 Durack, P. J., Taylor, K. E., Eyring, V., Ames, S., Hoang, T., Nadeau, D., Doutriaux, C., Stockhause, M., and Gleckler,  
761 P. J.: Toward standardized data sets for climate model experimentation, *Eos, Transactions American*  
762 *Geophysical Union*, 99, <https://doi.org/10.1029/2018eo101751>, 2018.

763 Eaton, B., Gregory, J., Drach, B., Taylor, K., Hankin, S., Blower, J., Caron, J., Signell, R., Bentley, P., Rappa, G.,  
764 Höck, H., Pamment, A., Juckes, M., Raspaud, M., Horne, R., Whiteaker, T., Blodgett, D., Zender, C., Lee,  
765 D., Hassell, D., Snow, A. D., Kölling, T., Allured, D., Jelenak, A., Soerensen, A. M., Gaultier, L., Herlédan,  
766 S.: NetCDF Climate and Forecast (CF) Meta-data Conventions V1.10, available at:  
767 <http://cfconventions.org/Data/cf-conventions/cf-conventions-1.10/cf-conventions.html> (last access: 4 April  
768 2024), 2022.

769 Eyring, V., Righi, M., Lauer, A., Evaldsson, M., Wenzel, S., Jones, C., Anav, A., Andrews, O., Cionni, I., Davin, E.  
770 L., Deser, C., Ehbrecht, C., Friedlingstein, P., Gleckler, P. J., Gottschaldt, K.-D., Hagemann, S., Juckes, M.,  
771 Kindermann, S., Krasting, J. P., Kunert, D., Levine, R. C., Loew, A., Mäkelä, J., Martin, G., Mason, E.,  
772 Phillips, A. S., Read, S., Rio, C., Roehrig, R., Senftleben, D., Sterl, A., Van Ulft, L. H., Walton, J., Wang,  
773 S., and Williams, K. D.: ESMValTool (v1.0) – a community diagnostic and performance metrics tool for  
774 routine evaluation of Earth system models in CMIP, *Geosic. Model Dev.*, 9, 1747–1802,  
775 <https://doi.org/10.5194/gmd-9-1747-2016>, 2016a.

776 Eyring, V., Bony, S., Meehl, G. A., A, C., Senior, Stevens, B., Stouffer, R. J., and Taylor, K. E.: Overview of the  
777 Coupled Model Intercomparison Project Phase 6 (CMIP6) experimental design and organization, *Geosic.*  
778 *Model Dev.*, 9, 1937–1958, <https://doi.org/10.5194/gmd-9-1937-2016>, 2016b.

779 Eyring, V., Cox, P. M., Flato, G. M., Gleckler, P. J., Abramowitz, G., Caldwell, P., Collins, W. D., Gier, B. K., Hall,  
780 A., Hoffman, F. M., Hurtt, G. C., Jahn, A., Jones, C. D., Klein, S. A., Krasting, J. P., Kwiatkowski, L.,  
781 Lorenz, R., Maloney, E. D., Meehl, G. A., Pendergrass, A. G., Pincus, R., Ruane, A. C., Russell, J. L.,  
782 Sanderson, B. M., Santer, B. D., Sherwood, S. C., Simpson, I. R., Stouffer, R. J., and Williamson, M. S.:

783 Taking climate model evaluation to the next level, *Nat. Clim. Change*, 9, 102–110,  
784 <https://doi.org/10.1038/s41558-018-0355-y>, 2019.

785 Eyring, V., Bock, L., Lauer, A., Righi, M., Schlund, M., Andela, B., Arnone, E., Bellprat, O., Brötz, B., Caron, L.-P.,  
786 Carvalhais, N., Cionni, I., Cortesi, N., Crezee, B., Davin, E. L., Davini, P., Debeire, K., De Mora, L., Deser,  
787 C., Docquier, D., Earnshaw, P., Ehbrecht, C., Gier, B. K., Gonzalez-Reviriego, N., Goodman, P. J.,  
788 Hagemann, S., Hardiman, S. C., Hassler, B., Hunter, A., Kadow, C., Kindermann, S., Koirala, S., Koldunov,  
789 N., Lejeune, Q., Lembo, V., Lovato, T., Lucarini, V., Massonnet, F., Müller, B., Pandde, A., Pérez-Zanón,  
790 N., Phillips, A. S., Predoi, V., Russell, J. L., Sellar, A., Serva, F., Stacke, T., Swaminathan, R., Torralba, V.,  
791 Vegas-Regidor, J., Von Hardenberg, J., Weigel, K., and Zimmermann, K.: Earth System Model Evaluation  
792 Tool (ESMValTool) v2.0 – an extended set of large-scale diagnostics for quasi-operational and  
793 comprehensive evaluation of Earth system models in CMIP, *Geosic. Model Dev.*, 13, 3383–3438,  
794 <https://doi.org/10.5194/gmd-13-3383-2020>, 2020.

795 Eyring, V., Gillett, N.P., Achuta Rao, K.M., Barimalala, R., Barreiro Parrillo, M., Bellouin, N., Cassou, C., Durack,  
796 P.J., Kosaka, Y., McGregor, S. and Min, S., Morgenstern, O., and Sun, Y.: Human Influence on the Climate  
797 System. In *Climate Change 2021: The Physical Science Basis. Contribution of Working Group I to the Sixth*  
798 *Assessment Report of the Intergovernmental Panel on Climate Change*. 105, 423-552,  
799 <https://doi.org/10.1017/9781009157896.005>, 2021.

800 Fasullo, J. T.: Evaluating simulated climate patterns from the CMIP archives using satellite and reanalysis datasets  
801 using the Climate Model Assessment Tool (CMATv1), *Geosic. Model Dev.*, 13, 3627–3642,  
802 <https://doi.org/10.5194/gmd-13-3627-2020>, 2020.

803 Fasullo, J. T., Phillips, A. S., and Deser, C.: Evaluation of leading modes of climate variability in the CMIP archives,  
804 *J. Climate*, 33, 5527–5545, <https://doi.org/10.1175/jcli-d-19-1024.1>, 2020.

805 Ferraro, R., Waliser, D. E., Gleckler, P. J., Taylor, K. E., and Eyring, V.: Evolving OBS4MIPS to support Phase 6 of  
806 the Coupled Model Intercomparison Project (CMIP6), *B. Am. Meteorol. Soc.*, [https://doi.org/10.1175/bams-](https://doi.org/10.1175/bams-d-14-00216.1)  
807 [d-14-00216.1](https://doi.org/10.1175/bams-d-14-00216.1), 2015.

808 Flato, G., Marotzke, J., Abiodun, B., Braconnot, P., Chou, S.C., Collins, W., Cox, P., Driouech, F., Emori, S., Eyring,  
809 V. and Forest, C.: Evaluation of climate models. In *Climate change 2013: the physical science basis. Contribution of Working Group I to the Fifth Assessment Report of the Intergovernmental Panel on Climate Change* (pp. 741-866). Cambridge University Press. 2014.

810 Fu, W., Moore, J. K., Primeau, F., Collier, N., Ogunro, O. O., Hoffman, F. M. and Randerson, J. T.: Evaluation of  
811 ocean biogeochemistry and carbon cycling in CMIP earth system models with the international ocean model  
812 benchmarking (IOMB) software System. *J. Geophys. Res.-Oceans*, 127, e2022JC018965,  
813 <https://doi.org/10.1029/2022JC018965>, 2022.

814  
815

816 Gates, W.L.: AN AMS continuing series: Global CHANGE–AMIP: The Atmospheric Model Intercomparison Project,  
817 *B. Am. Meteorol. Soc.*, 73, 1962-1970, 1992.

818 Gates, W.L., Henderson-Sellers, A., Boer, G.J., Folland, C.K., Kitoh, A., McAvaney, B.J., Semazzi, F., Smith, N.,  
819 Weaver, A.J. and Zeng, Q.C.: Climate models—evaluation. *Climate Change 1*: 229-284, 1995.

820 Gates, W.L., Boyle, J.S., Covey, C., Dease, C.G., Doutriaux, C.M., Drach, R.S., Fiorino, M., Gleckler, P.J., Hnilo,  
821 J.J., Marlais, S.M. and Phillips, T.J.: An overview of the results of the Atmospheric Model Intercomparison  
822 Project (AMIP I). *B. Am. Meteorol. Soc.*, 80, 29-56, 1999.

823 Gleckler, P. J., Taylor, K. E., and Doutriaux, C.: Performance metrics for climate models, *J. Geophys. Res.*, 113,  
824 <https://doi.org/10.1029/2007jd008972>, 2008.

825 Gleckler, P. J., Ferraro, R., and Waliser, D. E.: Improving use of satellite data in evaluating climate models, *Eos,*  
826 *Transactions American Geophysical Union*, 92, 172, <https://doi.org/10.1029/2011eo200005>, 2011.

827 Gleckler, P. J., Doutriaux, C., Durack, P. J., Taylor, K. E., Zhang, Y., Williams, D. N., Mason, E., and Servonnat, J.:  
828 A more powerful reality test for climate models, *Eos, Transactions American Geophysical Union*, 97,  
829 <https://doi.org/10.1029/2016eo051663>, 2016.

830 Golaz, J.-C., Caldwell, P., Van Roekel, L., Petersen, M. R., Tang, Q., Wolfe, J. D., Abeshu, G. W., Anantharaj, V.,  
831 Asay-Davis, X., Bader, D. C., Baldwin, S., Bisht, G., Bogenschutz, P., Branstetter, M. L., Brunke, M. A.,  
832 Brus, S., Burrows, S. M., Cameron-Smith, P. J., Donahue, A. S., Deakin, M., Easter, R. C., Evans, K. J.,  
833 Feng, Y., Flanner, M., Foucar, J. G., Fyke, J., Griffin, B. M., Hannay, C., Harrop, B. E., Hoffman, M. J.,  
834 Hunke, E., Jacob, R., Jacobsen, D. W., Jeffery, N., Jones, P. W., Keen, N. D., Klein, S. A., Larson, V. E.,  
835 Leung, L. R., Li, H. Y., Lin, W., Lipscomb, W. H., Lun, P., Mahajan, S., Maltrud, M., Mamatjanov, A.,  
836 McClean, J. L., McCoy, R., Neale, R., Price, S., Qian, Y., Rasch, P. J., Eyre, J. E. J. R., Riley, W. J., Ringler,  
837 T. D., Roberts, A., Roesler, E. L., Salinger, A. G., Shaheen, Z., Shi, X., Singh, B., Tang, J., Taylor, M. A.,  
838 Thornton, P. E., Turner, A. K., Veneziani, M., Wan, H., Wang, H., Wang, S., Williams, D. N., Wolfram, P.  
839 J., Worley, P. H., Xie, S., Yang, Y., Yoon, J., Zelinka, M. D., Zender, C. S., Zeng, X., Zhang, C., Zhang, K.,  
840 Zhang, Y., Zheng, X., Zhou, T., and Zhu, Q.: The DOE E3SM Coupled Model Version 1: Overview and  
841 evaluation at standard resolution, *J. Adv. Model. Earth Sy.*, 11, 2089–2129,  
842 <https://doi.org/10.1029/2018ms001603>, 2019.

843 Goldenson, N., Leung, L. R., Mearns, L. O., Pierce, D. W., Reed, K. A., Simpson, I. R., Ullrich, P., Krantz, W., Hall,  
844 A., Jones, A. and Rahimi, S.: Use-Inspired, Process-Oriented GCM Selection: Prioritizing Models for  
845 Regional Dynamical Downscaling, *B. Am. Meteorol. Soc.*, E1619–E1629, [https://doi.org/10.1175/BAMS-](https://doi.org/10.1175/BAMS-D-23-0100.1)  
846 [D-23-0100.1](https://doi.org/10.1175/BAMS-D-23-0100.1), 2023.

847 Guilyardi, E., Wittenberg, A., Fedorov, A., Collins, M., Wang, C., Capotondi, A., Van Oldenborgh, G.J. and  
848 Stockdale, T.: Understanding El Niño in ocean–atmosphere general circulation models: Progress and  
849 challenges, *B. Am. Meteorol. Soc.*, 90, 325-340, <https://doi.org/10.1175/2008BAMS2387.1>, 2009.

850 Guilyardi E., Capotondi, A., Lengaigne, M., Thual, S., Wittenberg, A. T.: ENSO modelling: history, progress and  
851 challenges, in: *El Niño in a changing climate*, edited by: McPhaden, M. J., Santoso, A., Cai, W., AGU  
852 monograph, ISBN: 9781119548164, <https://doi.org/10.1002/9781119548164.ch9>, 2020.

853 Gutowski Jr., W. J., Giorgi, F., Timbal, B., Frigon, A., Jacob, D., Kang, H.-S., Raghavan, K., Lee, B., Lennard, C.,  
854 Nikulin, G., O'Rourke, E., Rixen, M., Solman, S., Stephenson, T., and Tangang, F.: WCRP Coordinated  
855 Regional Downscaling EXperiment (CORDEX): a diagnostic MIP for CMIP6, *Geosci. Model Dev.*, 9, 4087–  
856 4095, <https://doi.org/10.5194/gmd-9-4087-2016>, 2016.

857 Haarsma, R. J., Roberts, M., Vidale, P. L., A. C., Senior, Bellucci, A., Bao, Q., Chang, P., Corti, S., Fučkar, N. S.,  
858 Guemas, V., Von Hardenberg, J., Hazeleger, W., Kodama, C., Koenigk, T., Leung, L. R., Lu, J., Luo, J.,  
859 Mao, J., Mizielinski, M. S., Mizuta, R., Nobre, P., Satoh, M., Scoccimarro, E., Semmler, T., Small, R. J., and  
860 Von Storch, J. S.: High Resolution Model Intercomparison Project (HiGHRESMIP v1.0) for CMIP6, *Geosic.*  
861 *Model Dev.*, 9, 4185–4208, <https://doi.org/10.5194/gmd-9-4185-2016>, 2016.

862 Hannah, W. M., Bradley, A. M., Guba, O., Tang, Q., Golaz, J.-C., and Wolfe, J. D.: Separating physics and dynamics  
863 grids for improved computational efficiency in spectral element Earth system models, *J. Adv. Model. Earth*  
864 *Sy.*, 13, <https://doi.org/10.1029/2020ms002419>, 2021.

865 Hassan, K. A., Rönnberg, N., Forsell, C., Cooper, M. and Johansson, J.: A study on 2D and 3D parallel coordinates  
866 for pattern identification in temporal multivariate data, in: 2019 23rd International Conference Information  
867 Visualisation (IV), 145-150, <https://doi.org/10.1109/IV.2019.00033>, 2019.

868 Hassell, D., Gregory, J. M., Blower, J., Lawrence, B., and Taylor, K. E.: A data model of the Climate and Forecast  
869 metadata conventions (CF-1.6) with a software implementation (cf-python v2.1), *Geosic. Model Dev.*, 10,  
870 4619–4646, <https://doi.org/10.5194/gmd-10-4619-2017>, 2017.

871 Hausfather, Z., Marvel, K., Schmidt, G. A., Nielsen-Gammon, J. W. and Zelinka, M.: Climate simulations: Recognize  
872 the ‘hot model’ problem, *Nature*, 605, 26-29, <https://doi.org/10.1038/d41586-022-01192-2>, 2022.

873 Held, I. M., Guo, H., Adcroft, A., Dunne, J. P., Horowitz, L. W., Krasting, J., Shevliakova, E., Winton, M., Zhao, M.,  
874 Bushuk, M., Wittenberg, A. T., and coauthors: Structure and performance of GFDL's CM4. 0 climate model,  
875 *J. Adv. Model. Earth Sy.*, 11, 3691-3727, <https://doi.org/10.1029/2019MS001829>, 2019.

876 Hendon, H. H., Zhang, C., and Glick, J. D.: Interannual Variation of the Madden–Julian Oscillation during Austral  
877 Summer, *J. Climate*, 12, 2538–2550, 1999.

878 Herger, N., Abramowitz, G., Knutti, R., Angélil, O., Lehmann, K., and Sanderson, B. M.: Selecting a climate model  
879 subset to optimise key ensemble properties, *Earth System Dynamics Discussions*, 9, 135–151,  
880 <https://doi.org/10.5194/esd-9-135-2018>, 2018.

881 Hersbach, H., Bell, B., Berrisford, P., Hirahara, S., Horányi, A., Muñoz-Sabater, J., Nicolas, J., Peubey, C., Radu, R.,  
882 Schepers, D. and coauthors: The ERA5 global reanalysis. *Q. J. Roy. Meteor. Soc.*, 146, 1999-2049,  
883 <https://doi.org/10.1002/qj.3803>, 2020.

884 Hintze, J. L., and Nelson, R. D.: Violin plots: A box plot-density trace synergism, *The American Statistician*, 52, 181–  
885 184, <https://doi.org/10.1080/00031305.1998.10480559>, 1998.

886 Hoyer, S. and Hamman, J.: xarray: N-D labeled Arrays and Datasets in Python, *J. Open Res. Software*, 5, 10.  
887 <https://doi.org/10.5334/jors.148>, 2017.

888 Huffman, G. J., Adler, R. F., Morrissey, M. M., Bolvin, D. T., Curtis, S., Joyce, R., McGavock, B. and Susskind, J.:  
889 Global precipitation at one-degree daily resolution from multisatellite observations, *J. Hydrometeorol.*, 2, 36-  
890 50, 2001.

891 Huffman, G. J., Bolvin, D. T., Braithwaite, D., Hsu, K., Joyce, R., Kidd, C., Nelkin, E. J., Sorooshian, S., Tan, J., and  
892 Xie, P.: NASA global precipitation measurement (GPM) integrated multi-satellite retrievals for GPM  
893 (IMERG). Algorithm theoretical basis document (ATBD) version, 4, p.30., 2015.

894 Inselberg, A.: Multidimensional detective, in: Proceedings of IEEE Symposium on Information Visualization, 100–  
895 107, <https://doi.org/10.1109/INFVIS.1997.636793>, 1997.

896 Inselberg, A.: Parallel Coordinates: Visualization, Exploration and Classification of High-Dimensional Data, in:  
897 Handbook of Data Visualization, edited by Chen, C., Härdle, W., and Unwin, A., Springer, Berlin,  
898 Heidelberg, Germany, 643-680, [https://doi.org/10.1007/978-3-540-33037-0\\_25](https://doi.org/10.1007/978-3-540-33037-0_25), 2008.

899 Inselberg, A.: Parallel Coordinates, in: Encyclopedia of Database Systems. Springer, edited by Liu, L., and Özsu, M.  
900 T., Springer, New York, NY, U.S.A., [https://doi.org/10.1007/978-1-4899-7993-3\\_262-2](https://doi.org/10.1007/978-1-4899-7993-3_262-2), 2016.

901 Johansson, J. and Forsell, C.: Evaluation of parallel coordinates: Overview, categorization and guidelines for future  
902 research, IEEE T. Vis. Comput. G. R., 22, 579-588, <https://doi.org/10.1109/TVCG.2015.2466992>, 2016.

903 Jakob, C., Gettelman, A. and Pitman, A.: The need to operationalize climate modelling, Nat. Clim. Chang. 13, 1158–  
904 1160, <https://doi.org/10.1038/s41558-023-01849-4>, 2023.

905 Joyce, R. J., Janowiak, J. E., Arkin, P. A. and Xie, P.: CMORPH: A method that produces global precipitation  
906 estimates from passive microwave and infrared data at high spatial and temporal resolution, J.  
907 Hydrometeorol., 5, 487-503, 2004.

908 Kang, D., Kim, D. H., Ahn, M.-S., Neale, R., Lee, J., and Gleckler, P. J.: The role of the mean state on MJO simulation  
909 in CESM2 ensemble simulation, Geophys. Res. Lett., 47, <https://doi.org/10.1029/2020gl089824>, 2020.

910 Kim, D., Sperber, K. R., Stern, W., Waliser, D. E., Kang, I. S., Maloney, E. D., Wang, W., Weickmann, K. M.,  
911 Benedict, J. J., Khairoutdinov, M., Lee, M.-I., Neale, R., Suarez, M. J., Thayer-Calder, K., and Zhang, G.:  
912 Application of MJO simulation diagnostics to climate models, J. Climate, 22, 6413–6436,  
913 <https://doi.org/10.1175/2009jcli3063.1>, 2009.

914 Kim, H., Caron, J. M., Richter, J. H. and Simpson, I. R.: The lack of QBO-MJO connection in CMIP6 models,  
915 Geophys. Res. Lett., 47, e2020GL087295, <https://doi.org/10.1029/2020GL087295>, 2020.

916 Klein, S. A., Zhang, Y., Zelinka, M. D., Pincus, R., Boyle, J., and Gleckler, P. J.: Are climate model simulations of  
917 clouds improving? An evaluation using the ISCCP simulator, J. Geophys. Res.-Atmos., 118, 1329–1342,  
918 <https://doi.org/10.1002/jgrd.50141>, 2013.

919 Klingaman, N. P., Martin, G., and Moise, A.: ASoP (v1.0): a set of methods for analyzing scales of precipitation in  
920 general circulation models, Geosic. Model Dev., 10, 57–83, <https://doi.org/10.5194/gmd-10-57-2017>, 2017.

921 Knutti, R.: The end of model democracy? Climatic Change, 102, 395–404, [https://doi.org/10.1007/s10584-010-9800-](https://doi.org/10.1007/s10584-010-9800-2)  
922 2, 2010.

923 Knutti, R., Sedláček, J., Sanderson, B. M., Lorenz, R., Fischer, E. M., and Eyring, V.: A climate model projection  
924 weighting scheme accounting for performance and interdependence, Geophys. Res. Lett.,  
925 <https://doi.org/10.1002/2016gl072012>, 2017.

926 Knutti, R., Abramowitz, G., Collins, M., Eyring, V., Gleckler, P. J., Hewitson, B., and Mearns, L.: Good Practice  
927 Guidance Paper on Assessing and Combining Multi Model Climate Projections, in: Meeting Report of the  
928 Intergovernmental Panel on Climate Change Expert Meeting on Assessing and Combining Multi Model  
929 Climate Projections, edited by Stocker, T. F., Qin, D., Plattner, G.-K., Tignor, M., and Midgley, P. M., IPCC  
930 Working Group I Technical Support Unit, University of Bern, Bern, Switzerland, 2010.

931 Labe, Z. M. and Barnes, E. A.: Comparison of Climate Model Large Ensembles With Observations in the Arctic Using  
932 Simple Neural Networks, *Earth and Space Science*, e2022EA002348,  
933 <https://doi.org/10.1029/2022EA002348>, 2022.

934 Lambert, S. J. and Boer, G. J.: CMIP1 evaluation and intercomparison of coupled climate models, *Clim. Dynam.*, 17,  
935 83-106, <https://doi.org/10.1007/PL00013736>, 2001.

936 Lee, H., Goodman, A., McGibbney, L. J., Waliser, D. E., Kim, J., Loikith, P. C., Gibson, P. B., and Massoud, E.:  
937 Regional Climate Model Evaluation System powered by Apache Open Climate Workbench v1.3.0: an  
938 enabling tool for facilitating regional climate studies, *Geosic. Model Dev.*, 11, 4435–4449,  
939 <https://doi.org/10.5194/gmd-11-4435-2018>, 2018a.

940 Lee, J., Ahn, M.-S., Ordonez, A., Gleckler, P., and Ullrich, P.: PCMDI/pcmdi\_metrics\_results\_archive, Zenodo [data],  
941 <https://doi.org/10.5281/zenodo.10181201>, 2023a.

942 Lee, J., Gleckler, P., Ordonez, A., Ahn, M.-S., Ullrich, P., Tom, V., Jason, B., Charles, D., Durack, P., Shaheen, Z.,  
943 Muryanto, L., Painter, J., and Krasting, J.: PCMDI/pcmdi\_metrics: PMP Version 3.1.1, Zenodo [code],  
944 <https://doi.org/10.5281/zenodo.592790>, 2023b.

945 Lee, J., Gleckler, P., Sperber, K., Doutriaux C., and Williams, D.: High-dimensional Data Visualization for Climate  
946 Model Intercomparison: Application of the Circular Plot, in: Proceedings of the 8th International Workshop  
947 on Climate Informatics: CI 2018. NCAR Technical Note NCAR/TN-550+PROC, 12-14,  
948 <http://dx.doi.org/10.5065/D6BZ64XQ>, 2018b.

949 Lee, J., Planton, Y., Gleckler, P. J., Sperber, K. R., Guilyardi, E., Wittenberg, A. T., McPhaden, M. J., and Pallotta,  
950 G.: Robust evaluation of ENSO in climate models: How many ensemble members are needed?, *Geophys.*  
951 *Res. Lett.*, 48, <https://doi.org/10.1029/2021gl095041>, 2021a.

952 Lee, J., Sperber, K. R., Gleckler, P. J., Bonfils, C., and Taylor, K. E.: Quantifying the agreement between observed  
953 and simulated extratropical modes of interannual variability, *Clim. Dynam.*, 52, 4057–4089,  
954 <https://doi.org/10.1007/s00382-018-4355-4>, 2019a.

955 Lee, J., Sperber, K. R., Gleckler, P. J., Taylor, K. E., and Bonfils, C.: Benchmarking performance changes in the  
956 simulation of extratropical modes of variability across CMIP generations, *J. Climate*, 1–70,  
957 <https://doi.org/10.1175/jcli-d-20-0832.1>, 2021b.

958 Lee, J., Xue, Y., De Sales, F., Diallo, I., Marx, L., Ek, M., Sperber, K. R., and Gleckler, P. J.: Evaluation of multi-  
959 decadal UCLA-CFSv2 simulation and impact of interactive atmospheric-ocean feedback on global and  
960 regional variability, *Clim. Dynam.*, 52, 3683–3707, <https://doi.org/10.1007/s00382-018-4351-8>, 2019b.

961 Leung, L. R., Boos, W. R., Catto, J. L., DeMott, C. A., Martin, G. M., Neelin, J. D., O’Brien, T. A., Xie, S., Feng, Z.,  
962 Klingaman, N. P. Kuo, Y.-H., Lee, R. W., Martinez-Villalobos, C., Vishnu S., Priestley, M. D. K., Tao, C.,  
963 and Zhou, Y.: Exploratory precipitation metrics: Spatiotemporal characteristics, process-oriented, and  
964 phenomena-based, *J. Climate*, 35, <https://doi.org/10.1175/JCLI-D-21-0590.1>, 3659-3686, 2022.

965 Lin, J.-P., Kiladis, G. N., Mapes, B. E., Weickmann, K. M., Sperber, K. R., Lin, W., Wheeler, M. C., Schubert, S. D.,  
966 Del Genio, A. D., Donner, L. J., Emori, S., Guérémy, J.-F., Hourdin, F., Rasch, P. J., Roeckner, E., and

967 Scinocca, J.: Tropical intraseasonal variability in 14 IPCC AR4 climate Models. Part I: Convective Signals,  
968 J. Climate, 19, 2665–2690, <https://doi.org/10.1175/jcli3735.1>, 2006.

969 Lin, Y., Huang, X., Liang, Y., Qin, Y., Xu, S., Huang, W., Xu, F., Liu, L., Wang, Y., Peng, Y. and Wang, L.:  
970 Community integrated earth system model (CIesm): Description and evaluation, J. Adv. Model. Earth Sy.,  
971 12, <https://doi.org/10.1029/2019ms002036>, 2020.

972 Loeb, N. G., Doelling, D. R., Wang, H., Su, W., Nguyen, C., Corbett, J. G., Liang, L., Mitrescu, C., Rose, F. G., and  
973 Seiji, K.: Clouds and the Earth's Radiant Energy System (CERES) Energy Balanced and Filled (EBAF) top-  
974 of-atmosphere (TOA) Edition-4.0 data product, International Journal of Climatology, 31, 895–918,  
975 <https://doi.org/10.1175/JCLI-D-17-0208.1>, 2018.

976 Longmate, J. M., Risser, M. D. and Feldman, D. R.: Prioritizing the selection of CMIP6 model ensemble members for  
977 downscaling projections of CONUS temperature and precipitation, Clim. Dyn., 61, 5171–5197,  
978 <https://doi.org/10.1007/s00382-023-06846-z>, 2023.

979 Lu, L., Wang, W. and Tan, Z.: Double-arc parallel coordinates and its axes re-ordering methods, Mobile Networks  
980 and Applications, 25, 1376-1391, <https://doi.org/10.1007/s11036-019-01455-9>, 2020.

981 Madden, R. A. and Julian, P.: Detection of a 40–50 day oscillation in the zonal wind in the Tropical Pacific, J. Atmos.  
982 Sci., 28, 702–708, [https://doi.org/10.1175/1520-0469\(1971\)028](https://doi.org/10.1175/1520-0469(1971)028), 1971.

983 Madden, R. A. and Julian, P.: Description of Global-Scale Circulation Cells in the Tropics with a 40–50 Day Period,  
984 J. Atmos. Sci., 29, 1109–1123, [https://doi.org/10.1175/1520-0469\(1972\)029](https://doi.org/10.1175/1520-0469(1972)029), 1972.

985 Madden, R. A. and Julian, P.: Observations of the 40–50-Day Tropical Oscillation—A Review, Mon. Weather Rev.,  
986 122, 814–837, [https://doi.org/10.1175/1520-0493\(1994\)122](https://doi.org/10.1175/1520-0493(1994)122), 1994.

987 Martin, G. M., Klingaman, N. P., and Moise, A. F.: Connecting spatial and temporal scales of tropical precipitation in  
988 observations and the MetUM-GA6, Geosic. Model Dev., 10, 105–126, [https://doi.org/10.5194/gmd-10-105-](https://doi.org/10.5194/gmd-10-105-2017)  
989 2017, 2017.

990 Maloney, E. D., Gettelman, A., Ming, Y., Neelin, J. D., Barrie, D., Mariotti, A., Chen, C., Coleman, D., Kuo, Y. H.,  
991 Singh, B., Annamalai, H., Berg, A., Booth, J. F., Camargo, S. J., Dai, A., Gonzalez, A., Hafner, J., Jiang, X.,  
992 Jing, X., Kim, D. H., Kumar, A., Moon, Y., Naud, C. M., Sobel, A. H., Suzuki, K., Wang, F., Wang, J., Wing,  
993 A. A., Xu, X., and Zhao, M.: Process-Oriented evaluation of climate and weather forecasting models, B. Am.  
994 Meteorol. Soc., 100, 1665–1686, <https://doi.org/10.1175/bams-d-18-0042.1>, 2019.

995 McAvaney, B.J., Covey, C., Joussaume, S., Kattsov, V., Kitoh, A., Ogana, W., Pitman, A.J., Weaver, A.J., Wood,  
996 R.A. and Zhao, Z.C.: Model evaluation. In Climate Change 2001: The scientific basis. Contribution of WG1  
997 to the Third Assessment Report of the IPCC (TAR) 471-523, Cambridge University Press, 2001.

998 McPhaden, M. J., Zebiak, S. E., and Glantz, M. H.: ENSO as an integrating concept in Earth Science, Science, 314,  
999 1740–1745, <https://doi.org/10.1126/science.1132588>, 2006.

1000 McPhaden, M. J., Santoso, A., Cai, W. (Eds.): El Niño Southern oscillation in a changing climate, American  
1001 Geophysical Union, USA, 528 pp., ISBN:9781119548126, <https://doi.org/10.1002/9781119548164>, 2020.



1002 Mears, C. A., Smith, D. K., Ricciardulli, L., Wang, J., Huelsing, H., & Wentz, F. J.: Construction and uncertainty  
1003 estimation of a satellite-derived total precipitable water data record over the world's oceans, *Earth and Space*  
1004 *Science*, 5, 197–210, <https://doi.org/10.1002/2018EA000363>, 2018.

1005 Meehl, G. A., Boer, G. J., Covey, C., Latif, M., and Stouffer, R. J.: The Coupled Model Intercomparison Project  
1006 (CMIP), *B. Am. Meteorol. Soc.*, 81, 313–318, 2000.

1007 Meehl, G. A., Boer, G. J., Covey, C., Latif, M., and Stouffer, R. J.: Intercomparison makes for a better climate model,  
1008 *Eos, Transactions American Geophysical Union*, 78, 445, <https://doi.org/10.1029/97eo00276>, 1997.

1009 Meehl, G. A., Covey, C., Delworth, T. L., Latif, M., McAvaney, B. J., Mitchell, J. F. B., Stouffer, R. J., and Taylor,  
1010 K. E.: THE WCRP CMIP3 Multimodel Dataset: A new era in climate change research, *B. Am. Meteorol.*  
1011 *Soc.*, 88, 1383–1394, <https://doi.org/10.1175/bams-88-9-1383>, 2007.

1012 Merrifield, A., Brunner, L., Lorenz, R., Humphrey, V., and Knutti, R.: Climate model Selection by Independence,  
1013 Performance, and Spread (ClimSIPS v1.0.1) for regional applications, *Geosic. Model Dev.*, 16, 4715–4747,  
1014 <https://doi.org/10.5194/gmd-16-4715-2023>, 2023.

1015 Neelin, J. D., Krasting, J. P., Radhakrishnan, A., Liptak, J., Jackson, T. J., Ming, Y., Dong, W., Gettelman, A.,  
1016 Coleman, D., Maloney, E. D., Wing, A. A., Kuo, Y. H., Ahmed, F., Ullrich, P. A., Bitz, C. M., Neale, R.,  
1017 Ordonez, A., and Maroon, E.: Process-oriented diagnostics: principles, practice, community development  
1018 and common standards, *B. Am. Meteorol. Soc.*, <https://doi.org/10.1175/bams-d-21-0268.1>, 2023.

1019 Nowack, P., Runge, J., Eyring, V., and Haigh, J. D.: Causal networks for climate model evaluation and constrained  
1020 projections, *Nat. Commun.*, 11, <https://doi.org/10.1038/s41467-020-15195-y>, 2020.

1021 Orbe, C., Van Roekel, L., Adames, Á. F., Dezfúli, A., Fasullo, J. T., Gleckler, P. J., Lee, J., Li, W., Nazarenko, L.,  
1022 Schmidt, G. A., Sperber, K. R., and Zhao, M.: Representation of modes of variability in six U.S. climate  
1023 models, *J. Climate*, 33, 7591–7617, <https://doi.org/10.1175/jcli-d-19-0956.1>, 2020.

1024 Ordonez, A. C., Klingaman, N. P., and Martin, G.: Analysing scales of precipitation, OSTI OAI (U.S. Department of  
1025 Energy Office of Scientific and Technical Information), <https://doi.org/10.11578/dc.20211029.5>, 2021.

1026 Papalexioú, S. M., Rajulapati, C. R., Clark, M. P., and Lehner, F.: Robustness of CMIP6 historical global mean  
1027 temperature simulations: Trends, long-term persistence, autocorrelation, and distributional shape, *Earth's*  
1028 *Future*, 8, e2020EF001667, <https://doi.org/10.1029/2020EF001667>, 2020.

1029 Pascoe, C., Lawrence, B. N., Guilyardi, E., Juckes, M., and Taylor, K. E.: Documenting numerical experiments in  
1030 support of the Coupled Model Intercomparison Project Phase 6 (CMIP6), *Geosci. Model Dev.*, 13, 2149–  
1031 2167, <https://doi.org/10.5194/gmd-13-2149-2020>, 2020.

1032 Pendergrass, A. G., Gleckler, P. J., Leung, L. R., and Jakob, C.: Benchmarking simulated precipitation in earth system  
1033 models, *B. Am. Meteorol. Soc.*, 101, E814–E816, <https://doi.org/10.1175/bams-d-19-0318.1>, 2020.

1034 Phillips, A. S., Deser, C., and Fasullo, J. T.: Evaluating modes of variability in climate models, *Eos, Transactions*  
1035 *American Geophysical Union*, 95, 453–455, <https://doi.org/10.1002/2014eo490002>, 2014.

1036 Planton, Y., Guilyardi, E., Wittenberg, A. T., Lee, J., Gleckler, P. J., Bayr, T., McGregor, S., McPhaden, M. J., Power,  
1037 S. B., Roehrig, R., Vialard, J., and Voldoire, A.: Evaluating Climate Models with the CLIVAR 2020 ENSO  
1038 Metrics Package, *B. Am. Meteorol. Soc.*, 102, E193–E217, <https://doi.org/10.1175/bams-d-19-0337.1>, 2021.

1039 Planton, Y. Y., Lee, J., Wittenberg, A. T., Gleckler, P. J., Guilyardi, E., McGregor, S., and McPhaden, M. J.: Estimating  
1040 uncertainty in simulated ENSO statistics, *J. Adv. Model. Earth Sy.* (under review), ESS Open Archive,  
1041 <https://doi.org/10.22541/essoar.170196744.48068128/v1>, 2023.

1042 Potter, G. L., Bader, D. C., Riches, M., Bamzai, A. and Joseph, R.: Celebrating two decades of the Program for Climate  
1043 Model Diagnosis and Intercomparison. *B. Am. Meteorol. Soc.*, 92, 629-631,  
1044 <https://doi.org/10.1175/2011BAMS3018.1>, 2011.

1045 Qin, Y., Zelinka, M. D., and Klein, S. A.: On the Correspondence Between Atmosphere-Only and Coupled  
1046 Simulations for Radiative Feedbacks and Forcing From CO<sub>2</sub>, *J. Geophys. Res.-Atmos.*, 127,  
1047 <https://doi.org/10.1029/2021jd035460>, 2022.

1048 Randall, D.A., Wood, R.A., Bony, S., Colman, R., Fichefet, T., Fyfe, J., Kattsov, V., Pitman, A., Shukla, J., Srinivasan,  
1049 J. and Stouffer, R.J.: Climate models and their evaluation. In *Climate change 2007: The physical science  
1050 basis. Contribution of Working Group I to the Fourth Assessment Report of the IPCC (FAR)*, 589-662,  
1051 Cambridge University Press, 2007.

1052 Randerson, J. T., Hoffman, F. M., Thornton, P. E., Mahowald, N. M., Lindsay, K., Lee, Y.-H., Nevison, C. D., Doney,  
1053 S. C., Bonan, G. B., Stöckli, R., Covey, C., Running, S. W., and Fung, I.: Systematic assessment of terrestrial  
1054 biogeochemistry in coupled climate-carbon models, *Glob. Change Biol.*, 15, 2462–2484,  
1055 <https://doi.org/10.1111/j.1365-2486.2009.01912.x>, 2009.

1056 Rasch, P. J., Xie, S., Ma, P.-L., Lin, W., Wang, H., Tang, Q., Burrows, S. M., Caldwell, P., Zhang, K., Easter, R. C.,  
1057 Cameron-Smith, P. J., Singh, B., Wan, H., Golaz, J.-C., Harrop, B. E., Roesler, E. L., Bacmeister, J. T.,  
1058 Larson, V. E., Evans, K. J., Qian, Y., Taylor, M. A., Leung, L. R., Zhang, Y., Brent, L., Branstetter, M. L.,  
1059 Hannay, C., Mahajan, S., Mamatjanov, A., Neale, R., Richter, J. H., Yoon, J.-H., Zender, C. S., Bader, D. C.,  
1060 Flanner, M., Foucar, J. G., Jacob, R., Keen, N. D., Klein, S. A., Liu, X., Salinger, A. G., Shrivastava, M., and  
1061 Yang, Y.: An overview of the atmospheric component of the Energy Exascale Earth System model, *J. Adv.  
1062 Model. Earth Sy.*, 11, 2377–2411, <https://doi.org/10.1029/2019ms001629>, 2019.

1063 Reichler, T. and Kim, J.: How well do coupled models simulate today’s climate?, *B. Am. Meteorol. Soc.*, 89, 303–  
1064 312, <https://doi.org/10.1175/bams-89-3-303>, 2008.

1065 Righi, M., Andela, B., Eyring, V., Lauer, A., Predoi, V., Schlund, M., Vegas-Regidor, J., Bock, L., Brötz, B., De  
1066 Mora, L., Diblen, F., Dreyer, L., Drost, N., Earnshaw, P., Hassler, B., Koldunov, N., Little, B., Tomas, S. L.,  
1067 and Zimmermann, K.: Earth System Model Evaluation Tool (ESMValTool) v2.0 – technical overview,  
1068 *Geosic. Model Dev.*, 13, 1179–1199, <https://doi.org/10.5194/gmd-13-1179-2020>, 2020.

1069 Sanderson, B. M. and Wehner, M. F.: Weighting strategy for the Fourth National Climate Assessment, in: *Climate  
1070 Science Special Report: Fourth National Climate Assessment, Volume I*, edited by Wuebbles, D. J., Fahey,  
1071 D. W., Hibbard, K. A., Dokken, D. J., Stewart, B. C., and Maycock, T.K., U.S. Global Change Research  
1072 Program, Washington, DC, USA, 436-442, <https://doi.org/10.7930/J06T0JS3>, 2017.

1073 Sanderson, B. M., Wehner, M., and Knutti, R.: Skill and independence weighting for multi-model assessments,  
1074 *Geosic. Model Dev.*, 10, 2379–2395, <https://doi.org/10.5194/gmd-10-2379-2017>, 2017.

1075 Sherwood, S. C., Webb, M. J., Annan, J. D., Armour, K. C., Forster, P. M., Hargreaves, J. C., Hegerl, G. C., Klein, S.  
1076 A., Marvel, K., Rohling, E. J., Watanabe, M., Andrews, T., Braconnot, P., Bretherton, C. S., Foster, G. L.,  
1077 Hausfather, Z., Von Der Heydt, A. S., Knutti, R., Mauritsen, T., Norris, J. R., Proistosescu, C., Rugenstein,  
1078 M., Schmidt, G. A., Tokarska, K., and Zelinka, M. D.: An assessment of Earth's climate sensitivity using  
1079 multiple lines of evidence, *Rev. Geophys.*, 58, <https://doi.org/10.1029/2019rg000678>, 2020.

1080 Singh, R., and AchutaRao, K.: Sensitivity of future climate change and uncertainty over India to performance-based  
1081 model weighting. *Clim. Change*, <https://doi.org/10.1007/s10584-019-02643-y>, 2020.

1082 Sillmann, J., Kharin, V. V., Zhang, X., Zwiers, F. W., and Bronaugh, D.: Climate extremes indices in the CMIP5  
1083 multimodel ensemble: Part 1. Model evaluation in the present climate, *J. Geophys. Res.-Atmos.*, 118, 1716–  
1084 1733, <https://doi.org/10.1002/jgrd.50203>, 2013.

1085 Sperber, K. R.: Madden-Julian variability in NCAR CAM2.0 and CCSM2.0, *Clim. Dyn.*, 23, 259–278,  
1086 <https://doi.org/10.1007/s00382-004-0447-4>, 2004.

1087 Sperber, K. R., Annamalai, H., Kang, I.-S., Kitoh, A., Moise, A., Turner, A., Wang, B., and Zhou, T.: The Asian  
1088 summer monsoon: an intercomparison of CMIP5 vs. CMIP3 simulation of the late 20th century. *Clim. Dyn.*,  
1089 41, 2711–2744, <https://doi.org/10.1007/s00382-012-1607-6>, 2013.

1090 Sperber K. R., Gualdi, S., Legutke, S., Gayler, V.: The Madden–Julian oscillation in ECHAM4 coupled and uncoupled  
1091 general circulation models, *Clim. Dyn.*, 25, 117–140, <https://doi.org/10.1007/s00382-005-0026-3>, 2005.

1092 Srivastava, A., Grotjahn, R., and Ullrich, P. A.: Evaluation of historical CMIP6 model simulations of extreme  
1093 precipitation over contiguous US regions, *Weather and Climate Extremes*, 29, 100268,  
1094 <https://doi.org/10.1016/j.wace.2020.100268>, 2020.

1095 Steed, C. A., Shipman, G., Thornton, P., Ricciuto, D., Erickson, D. and Branstetter, M.: Practical application of parallel  
1096 coordinates for climate model analysis, *Procedia Comput. Sci.*, 9, 877–886,  
1097 <https://doi.org/10.1016/j.procs.2012.04.094>, 2012.

1098 Stevens, B., Satoh, M., Auger, L., Biercamp, J., Bretherton, C. S., Chen, X., Düben, P., Judt, F., Khairoutdinov, M.,  
1099 Klocke, D., Kodama, C., Kornblueh, L., Lin, S.-J., Neumann, P., Putman, W. M., Röber, N., Shibuya, R.,  
1100 Vanniere, B., Vidale, P. L., Wedi, N., and Zhou, L.: DYAMOND: the DYnamics of the Atmospheric general  
1101 circulation Modeled On Non-hydrostatic Domains, *Progress in Earth and Planetary Science*, 6,  
1102 <https://doi.org/10.1186/s40645-019-0304-z>, 2019.

1103 Stoner, A. M. K., Hayhoe, K., and Wuebbles, D. J.: Assessing general circulation model simulations of atmospheric  
1104 teleconnection patterns, *J. Climate*, 22, 4348–4372, <https://doi.org/10.1175/2009jcli2577.1>, 2009.

1105 Sung, H. M., Kim, J., Shim, S., Seo, J., Kwon, S.-H., Sun, M.-A., Moon, H.-J., Lee, J., Lim, Y. C., Boo, K.-O., Kim,  
1106 Y., Lee, J., Lee, J., Kim, J.-S., Marzin, C., and Byun, Y.-H.: Climate change projection in the Twenty-First  
1107 Century simulated by NIMS-KMA CMIP6 model based on new GHGs concentration pathways, *Asia-Pac. J.*  
1108 *Atmos. Sci.*, 57, 851–862, <https://doi.org/10.1007/s13143-021-00225-6>, 2021.

1109 Tang, Q., Prather, M. J., Hsu, J., Ruiz, D. J., Cameron-Smith, P. J., Xie, S., and Golaz, J.-C.: Evaluation of the  
1110 interactive stratospheric ozone (O3v2) module in the E3SM version 1 Earth system model, *Geosic. Model*  
1111 *Dev.*, 14, 1219–1236, <https://doi.org/10.5194/gmd-14-1219-2021>, 2021.

1112 Tang, S., Fast, J. D., Zhang, K., Hardin, J. C., Varble, A. C., Shilling, J. E., Mei, F., Zawadowicz, M. A., and Ma, P.-  
1113 L.: Earth System Model Aerosol–Cloud Diagnostics (ESMAC Diags) package, version 1: assessing E3SM  
1114 aerosol predictions using aircraft, ship, and surface measurements, *Geosci. Model Dev.*, 15, 4055–4076,  
1115 <https://doi.org/10.5194/gmd-15-4055-2022>, 2022.

1116 Tang, S., Varble, A. C., Fast, J. D., Zhang, K., Wu, P., Dong, X., Mei, F., Pekour, M., Hardin, J. C., and Ma, P.-L.:  
1117 Earth System Model Aerosol–Cloud Diagnostics (ESMAC Diags) package, version 2: assessing aerosols,  
1118 clouds, and aerosol–cloud interactions via field campaign and long-term observations, *Geosci. Model Dev.*,  
1119 16, 6355–6376, <https://doi.org/10.5194/gmd-16-6355-2023>, 2023.

1120 Taylor, K. E.: Truly Conserving with Conservative Remapping Methods, *Geosci. Model Dev.* 17, 415–430,  
1121 <https://doi.org/10.5194/gmd-17-415-2024>, 2024.

1122 Taylor, K. E.: Summarizing multiple aspects of model performance in a single diagram, *J. Geophys. Res.*, 106, 7183–  
1123 7192, <https://doi.org/10.1029/2000jd900719>, 2001.

1124 Taylor, K. E., Stouffer, R. J., and Meehl, G. A.: An overview of CMIP5 and the experiment design, *B. Am. Meteorol.*  
1125 *Soc.*, 93, 485–498, <https://doi.org/10.1175/bams-d-11-00094.1>, 2012.

1126 Teixeira, J., Waliser, D. E., Ferraro, R., Gleckler, P. J., Lee, T., and Potter, G. L.: Satellite observations for CMIP5:  
1127 The Genesis of OBS4MIPs, *B. Am. Meteorol. Soc.*, 95, 1329–1334, [https://doi.org/10.1175/bams-d-12-](https://doi.org/10.1175/bams-d-12-00204.1)  
1128 00204.1, 2014.

1129 Tian, B., and Dong, X.: The Double-ITCZ Bias in CMIP3, CMIP5, and CMIP6 Models Based on Annual Mean  
1130 Precipitation, *Geophys. Res. Lett.*, 47, e2020GL087232, <https://doi.org/10.1029/2020GL087232>, 2020

1131 Ullrich, P. A. and Zarzycki, C. M.: TempestExtremes: a framework for scale-insensitive pointwise feature tracking on  
1132 unstructured grids, *Geosci. Model Dev.*, 10, 1069–1090, <https://doi.org/10.5194/gmd-10-1069-2017>, 2017.

1133 Ullrich, P. A., Zarzycki, C. M., McClenny, E., Pinheiro, M. C., Stansfield, A. M., and Reed, K. A.: TempestExtremes  
1134 v2.1: a community framework for feature detection, tracking, and analysis in large datasets, *Geosci. Model*  
1135 *Dev.*, 14, 5023–5048, <https://doi.org/10.5194/gmd-14-5023-2021>, 2021.

1136 U.S. Department of Energy (DOE): Benchmarking Simulated Precipitation in Earth System Models Workshop Report,  
1137 DOE/SC-0203, U.S. Department of Energy Office of Science, Biological and Environmental Research (BER)  
1138 Program. Germantown, Maryland, USA. 2020.

1139 Vo, T., Po-Chedley, P., Boutte, J., Zhang, C., Lee, J., Gleckler, P., Durack, P., Taylor, K., and Golaz, J.-C.: Xarray  
1140 Climate Data Analysis Tools (xCDAT): A Python Package for Simple and Robust Analysis of Climate Data,  
1141 The 103rd AMS Annual Meeting, Abstract, 2023.

1142 Waliser, D. E., Gleckler, P. J., Ferraro, R., Taylor, K. E., Ames, S., Biard, J., Bosilovich, M. G., Brown, O. B., Chepfer,  
1143 H., Cinquini, L., Durack, P. J., Eyring, V., Mathieu, P.-P., Lee, T., Pinnock, S., Potter, G. L., Rixen, M.,  
1144 Saunders, R., Schulz, J. B., Thépaut, J.-N., and Tuma, M.: Observations for Model Intercomparison Project  
1145 (Obs4MIPs): status for CMIP6, *Geosci. Model Dev.*, 13, 2945–2958, [https://doi.org/10.5194/gmd-13-2945-](https://doi.org/10.5194/gmd-13-2945-2020)  
1146 2020, 2020.

1147 Waliser, D. E., Sperber, K. R., Hendon, H. H., Kim, D., Maloney, E. D., Wheeler, M. C., Weickmann, K. M., Zhang,  
1148 C., Donner, L. J., Gottschalck, J., Higgins, W., Kang, I. S., Legler, D. M., Moncrieff, M. W., Schubert, S. D.,

1149 Stern, W., Vitart, F., Wang, B., Wang, W., and Woolnough, S. J.: MJO Simulation Diagnostics, *J. Climate*,  
1150 22, 3006–3030, <https://doi.org/10.1175/2008jcli2731.1>, 2009.

1151 Wang, J., Liu, X., Shen, H. W. and Lin, G.: Multi-resolution climate ensemble parameter analysis with nested parallel  
1152 coordinates plots, *IEEE T. Vis. Comput. G. R.*, 23, 81-90, <https://doi.org/10.1109/TVCG.2016.2598830>,  
1153 2017.

1154 Wehner, M., Gleckler, P. J., and Lee, J.: Characterization of long period return values of extreme daily temperature  
1155 and precipitation in the CMIP6 models: Part 1, model evaluation, *Weather and Climate Extremes*, 30,  
1156 100283, <https://doi.org/10.1016/j.wace.2020.100283>, 2020.

1157 Wehner, M., Lee, J., Risser, M. D., Ullrich, P. A., Gleckler, P. J., and Collins, W. D.: Evaluation of extreme sub-daily  
1158 precipitation in high-resolution global climate model simulations, *Philos. T. R. Soc. A.*, 379, 20190545,  
1159 <https://doi.org/10.1098/rsta.2019.0545>, 2021.

1160 Williams, D. N.: Visualization and analysis tools for ultrascale climate data, *Eos, Transactions American Geophysical*  
1161 *Union*, 95, 377–378, <https://doi.org/10.1002/2014eo420002>, 2014.

1162 Williams, D. N., Balaji, V., Cinquini, L., Denvil, S., Duffy, D. Q., Evans, B., Ferraro, R., Hansen, R., Lautenschlager,  
1163 M., and Trenham, C.: A global repository for Planet-Sized experiments and observations, *B. Am. Meteorol.*  
1164 *Soc.*, 97, 803–816, <https://doi.org/10.1175/bams-d-15-00132.1>, 2016.

1165 Williams, D. N., Doutriaux, C., Drach, R., and McCoy, R.: The Flexible Climate Data Analysis Tools (CDAT) for  
1166 Multi-model Climate Simulation Data, *IEEE International Conference on Data Mining Workshops*, 254–261,  
1167 <https://doi.org/10.1109/icdmw.2009.64>, 2009.

1168 Wong, P. C., Shen, H. W., Leung, R., Hagos, S., Lee, T. Y., Tong, X. and Lu, K.: Visual analytics of large-scale  
1169 climate model data, in: 2014 IEEE 4th Symposium on Large Data Analysis and Visualization (LDAV), 85-  
1170 92, <https://doi.org/10.1109/LDAV.2014.7013208>, 2014.

1171 Xie, P., Joyce, R., Wu, S., Yoo, S.H., Yarosh, Y., Sun, F. and Lin, R.: Reprocessed, bias-corrected CMORPH global  
1172 high-resolution precipitation estimates from 1998, *J. Hydrometeorol.*, 18, 1617-1641, 2017.

1173 Xue, Z. and Ullrich, P. A.: A Comprehensive Intermediate-Term Drought Evaluation System and Evaluation of  
1174 Climate Data Products over the Conterminous United States, *J. Hydrometeorol.*, <https://doi.org/10.1175/jhmd-20-0314.1>, 2021.

1176 Young, A. H., Knapp, K. R., Inamdar, A. K., Hankins, W., and Rossow, W. B.: The International Satellite Cloud  
1177 Climatology Project H-Series climate data record product, *Earth Syst. Sci. Data*, 10, 583–593,  
1178 <https://doi.org/10.5194/essd-10-583-2018>, 2018.

1179 Zelinka, M. D., Klein, S. A., Qin, Y., and Myers, T. A.: Evaluating climate models’ cloud feedbacks against expert  
1180 judgment, *J. Geophys. Res.-Atmos.*, 127, <https://doi.org/10.1029/2021jd035198>, 2022.

1181 Zelinka, M. D., Myers, T. A., McCoy, D. T., Po-Chedley, S., Caldwell, P. M., Ceppi, P., Klein, S. A., and Taylor, K.  
1182 E.: Causes of higher climate sensitivity in CMIP6 models, *Geophys. Res. Lett.*, 47, e2019GL085782,  
1183 <https://doi.org/10.1029/2019GL085782>, 2020.

1184 Zhang, C., Golaz, J.-C., Forsyth, R., Vo, T., Xie, S., Shaheen, Z., Potter, G. L., Asay-Davis, X. S., Zender, C. S., Lin,  
1185 W., Chen, C.-C., Terai, C. R., Mahajan, S., Zhou, T., Balaguru, K., Tang, Q., Tao, C., Zhang, Y.,

1186 Emmenegger, T., Burrows, S., and Ullrich, P. A.: The E3SM Diagnostics Package (E3SM Diags v2.7): a  
1187 Python-based diagnostics package for Earth system model evaluation, *Geosci. Model Dev.*, 15, 9031–9056,  
1188 <https://doi.org/10.5194/gmd-15-9031-2022>, 2022.

1189 Zhang, C. and Hendon, H. H.: Propagating and standing components of the intraseasonal oscillation in tropical  
1190 convection, *J. Atmos. Sci.*, 54, 741–752, [https://doi.org/10.1175/1520-0469\(1997\)054](https://doi.org/10.1175/1520-0469(1997)054), 1997.

1191 Zhang, C., Xie, S., Klein, S. A., Ma, H. Y., Tang, S., Van Weverberg, K., Morcrette, C. J. and Petch, J.: CAUSES:  
1192 Diagnosis of the summertime warm bias in CMIP5 climate models at the ARM Southern Great Plains site.  
1193 *J. Geophys. Res.-Atmos.*, 123, 2968-2992, <https://doi.org/10.1002/2017JD027200>, 2018.

1194 Zhang, C., Xie, S., Tao, C., Tang, S., Emmenegger, T., Neelin, J. D., Schiro, K. A., Lin, W. and Shaheen, Z.: The  
1195 ARM data-oriented metrics and diagnostics package for climate models: A new tool for evaluating climate  
1196 models with field data, <https://doi.org/10.1175/BAMS-D-19-0282.1>, *B. Am. Meteorol. Soc.*, 101, E1619-  
1197 E1627, 2020.

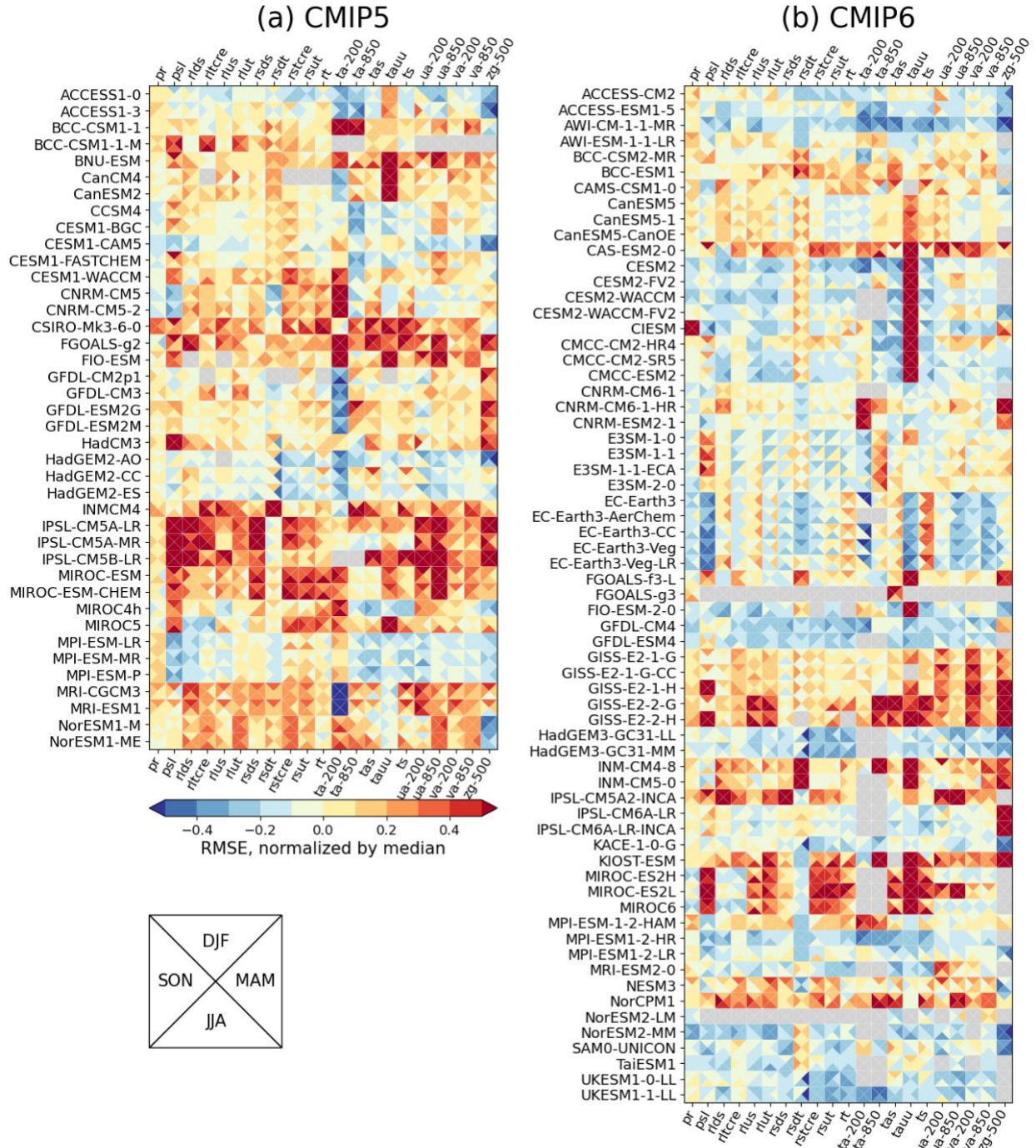
1198 Zhao, B., Lin, P., Hu, A., Liu, H., Ding, M., Yu, Z., and Yu, Y.: Uncertainty in Atlantic Multidecadal Oscillation  
1199 derived from different observed datasets and their possible causes, *Frontiers in Marine Science*, 9,  
1200 <https://doi.org/10.3389/fmars.2022.1007646>, 2022.

1201 Zhao, M., Golaz, J.-C., Held, I. M., Guo, H., Balaji, V., Benson, R., Chen, J. H., Chen, X., Donner, L. J., Dunne, J.,  
1202 Dunne, K. A., Durachta, J., Fan, S.-M., Freidenreich, S. M., Garner, S. T., Ginoux, P., Harris, L., Horowitz,  
1203 L. W., Krasting, J. P., Langenhorst, A. R., Zhi, L., Lin, P., Lin, S. J., Malyshev, S., Mason, E., Milly, P. C.  
1204 D., Ming, Y., Naik, V., Paulot, F., Paynter, D., Phillipps, P. J., Radhakrishnan, A., Ramaswamy, V.,  
1205 Robinson, T., Schwarzkopf, D., Seman, C. J., Shevliakova, E., Shen, Z., Shin, H. H., Silvers, L. G., Wilson,  
1206 J. R., Winton, M., Wittenberg, A. T., Wyman, B., and Xiang, B.: The GFDL Global Atmosphere and Land  
1207 Model AM4.0/LM4.0: 1. Simulation characteristics with prescribed SSTs, *J. Adv. Model. Earth Sy.*, 10,  
1208 691–734, <https://doi.org/10.1002/2017ms001208>, 2018.

1209

1210 **Table 1.** List of variables and observation datasets used as reference datasets for the PMP's  
 1211 mean climate evaluation in this paper (Sect. 3.1 and Figs. 1-2). A ditto mark (") indicates the  
 1212 same as above.  
 1213

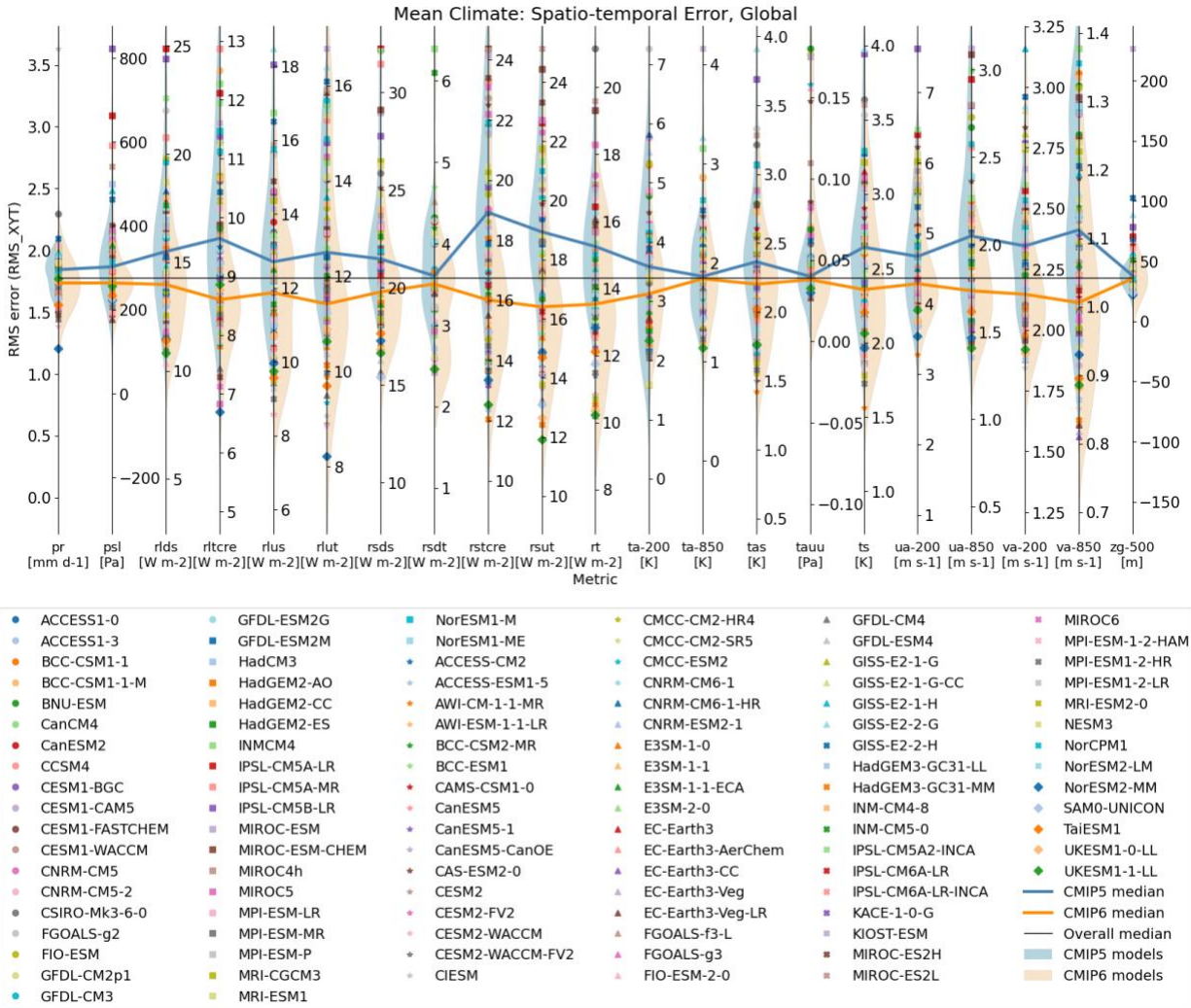
Variable	Variable full name	Product	Reference
ps	Precipitation	GPCP-2-3	Adler et al. (2018)
psl	Sea level pressure	ERA-5	Hersbach et al. (2020)
rlds	Surface Downwelling Longwave Radiation	CERES-EBAF-4-1	Loeb et al. (2018)
rltcre	Longwave cloud radiative effect	"	
rlus	Surface Upwelling Longwave Radiation	"	
rlut	Upwelling longwave at the top of atmosphere	"	
rsds	Surface Downwelling Shortwave Radiation	"	
rsdt	TOA Incident Shortwave Radiation	"	
rstcre	Shortwave cloud radiative effect	"	
rsut	Upwelling shortwave at the top of atmosphere	"	
rt	Net radiative flux	"	
ta-200, ta-850	Air temperature at 850 and 200 hPa	ERA-5	Hersbach et al. (2020)
tas	2-m air temperature	"	
tauu	Surface zonal wind stress	ERA-INT	Dee et al. (2011)
ts	Surface temperature	ERA-5	Hersbach et al. (2020)
ua-200, ua-850	Zonal wind component at 850 and 200 hPa	"	
va-200, va-850	Meridional wind component at 850 and 200 hPa	"	
zg-500	Geopotential height at 500 hPa	"	



1214  
 1215 **Figure 1.** Portrait plot for spatial RMSE (uncentered) of global seasonal climatologies for (a)  
 1216 CMIP5 (models ACCESS1-0 to NorESM1-ME on the ordinate) and (b) CMIP6 (models  
 1217 ACCESS-CM2 to UKESM1-1-LL on the ordinate) for 1981-2005 epoch. The RMSE is calculated  
 1218 for each season (shown as triangles in each box) over the globe including both land and ocean,  
 1219 and model and reference data were interpolated to a common 2.5x2.5 degree grid. The RMSE  
 1220 of each variable is normalized by the median RMSE of all CMIP5 and 6 models. A result of 0.2  
 1221 (-0.2) is indicative of an error that is 20% greater (lesser) than the median RMSE across all  
 1222 models. Models in each group are sorted in alphabetical order. Full names of variable names on  
 1223 the abscissa and their reference datasets can be found in Table 1. Detailed information for



1224 models can be found at the *Earth System Documentation* (ES-DOC, <https://search.es-doc.org/>;  
1225 Pascoe et al., 2020). The interactive version of the Portrait plot in this figure is available on the  
1226 PMP result pages on the PCMDI website ([https://pcmdi.llnl.gov/metrics/mean\\_clim/](https://pcmdi.llnl.gov/metrics/mean_clim/)).



1227  
 1228  
 1229  
 1230  
 1231  
 1232  
 1233  
 1234  
 1235  
 1236  
 1237  
 1238  
 1239

**Figure 2.** Parallel Coordinate Plot for spatio-temporal RMSE (Gleckler et al., 2008) from mean climate evaluation. Each vertical axis represents a different variable. Results from each model are displayed as symbols. Middle of each vertical axis is aligned with the median statistic of all CMIP5 and CMIP6 models. The cross-generation model distributions of model performance are shaded on the left (CMIP5, blue) and right (CMIP6, orange) sides of each axis. Also, medians from CMIP5 (blue) and CMIP6 (orange) model groups are highlighted as lines. Full names for model variables on the abscissa and their reference datasets can be found in Table 1. Time epoch used for this analysis is 1981-2005. Detailed information for models can be found at the *Earth System Documentation* (ES-DOC, <https://search.es-doc.org/>; Pascoe et al., 2020). The interactive version of the Portrait plot in this figure is available on the PMP result pages on the PCMDI website ([https://pcmdi.llnl.gov/metrics/mean\\_clim/](https://pcmdi.llnl.gov/metrics/mean_clim/)).



1240  
 1241 **Figure 3.** Application of ENSO metrics to CMIP6 models. Model names with an asterisk (\*)  
 1242 indicate that 10 or more ensemble members were used in this analysis. Dots indicate metric  
 1243 values from individual ensemble members while bars indicate the average of metric values  
 1244 across the ensemble members. Bars colored for easier identification of model names at the  
 1245 bottom of the figure. Metrics were grouped into three *Metric Collections*: (a-n) ENSO  
 1246 Performance, (o-r) ENSO Teleconnections, and (s-w) ENSO processes. Names of individual  
 1247 metrics and default reference datasets being used are noted on top of each panel, and  
 1248 observational uncertainty by applying the metrics for alternative reference datasets noted on the  
 1249 upper right of each panel is shown as gray-shaded. Detailed descriptions for each metric can be  
 1250 found at [https://github.com/CLIVAR-PRP/ENSO\\_metrics/wiki](https://github.com/CLIVAR-PRP/ENSO_metrics/wiki).

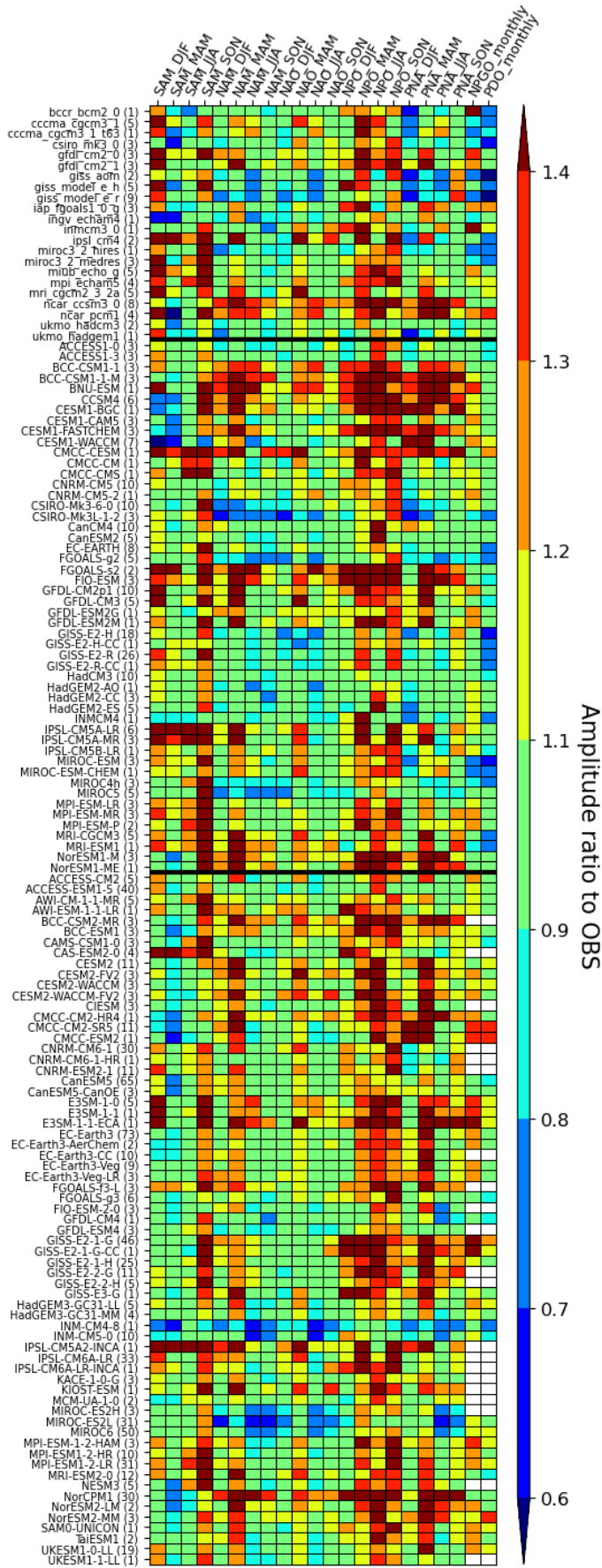
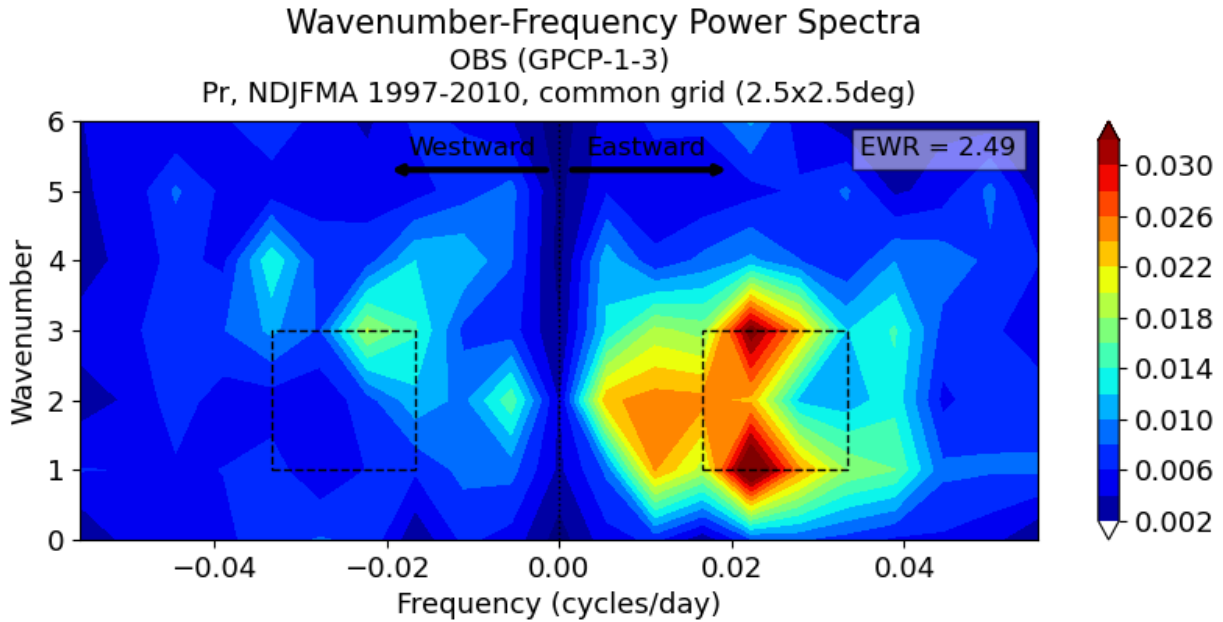
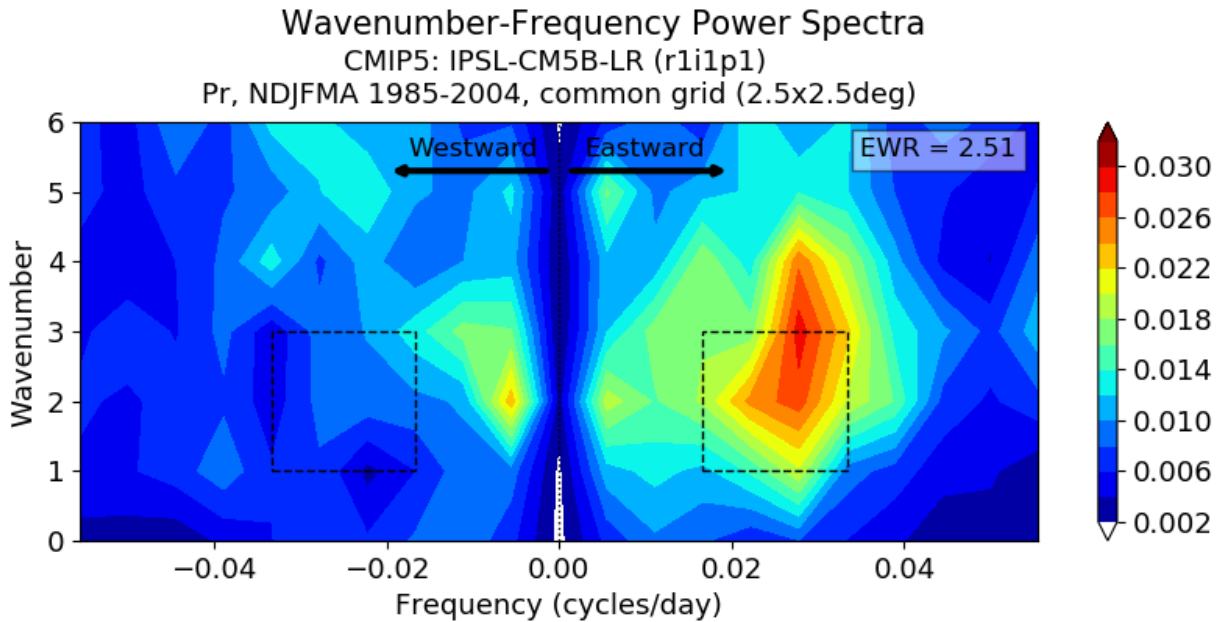


**Figure 4.** Portrait plots of the amplitude of extratropical modes of variability simulated by CMIP3, 5, and 6 models in their historical or equivalent simulations, as gauged by the ratio of spatiotemporal standard deviations of the model and observed PCs, obtained using the CBF method in the PMP. Columns (horizontal axis) are for mode and season, and rows (vertical axis) are for models from CMIP3 (top), CMIP5 (middle), and CMIP6 (bottom), separated by thick black horizontal lines. For sea level pressure–based modes (SAM, NAM, NAO, NPO, and PNA) in the upper-left hand triangle the model results are shown relative to NOAA-20CR. For SST-based modes (NPGO and PDO), results are shown relative to HadISSTv1.1. Numbers in parentheses following model names indicate the number of ensemble members for the model. Metrics for individual ensemble members were averaged for each model. White boxes indicate missing value.

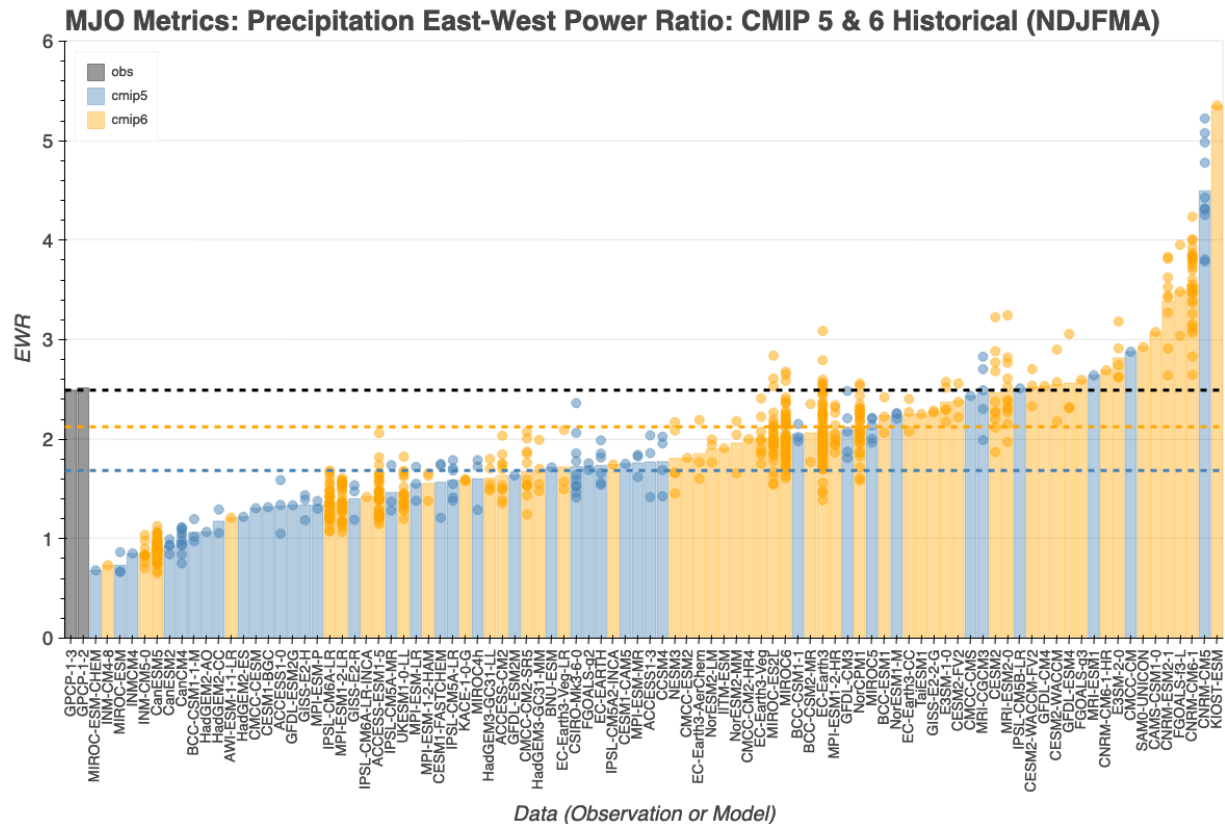
1277  
1278 (a) Observation



1279  
1280 (b) Model

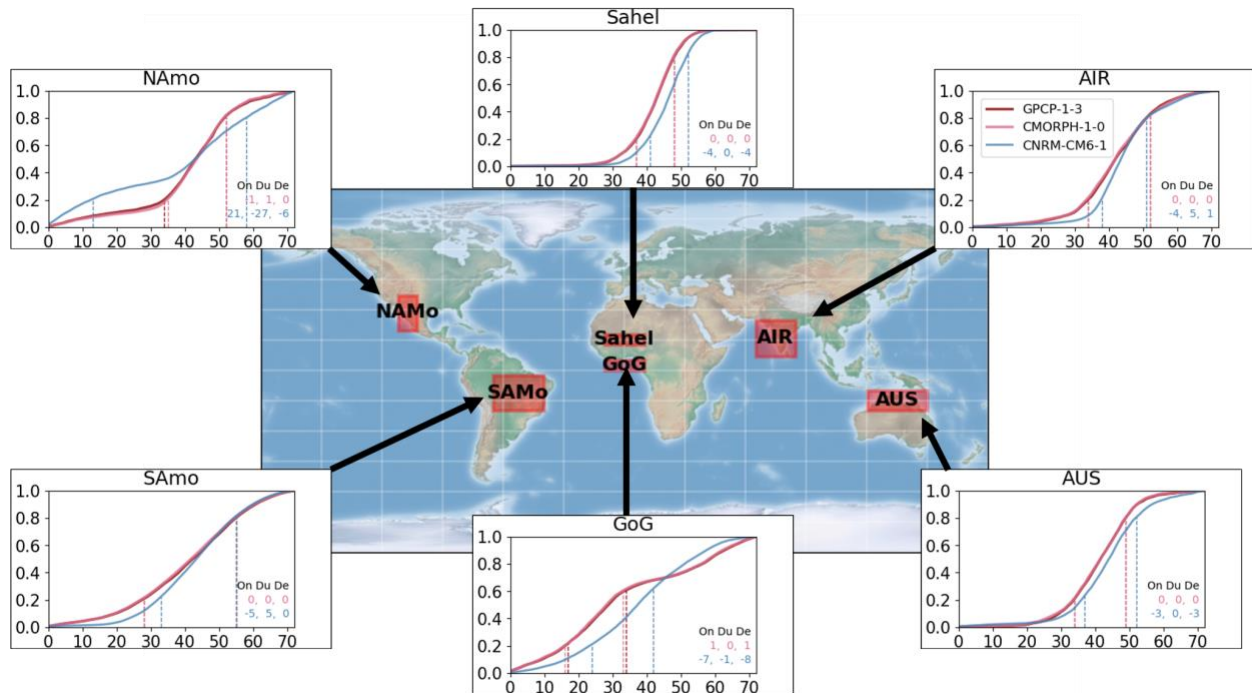


1281  
1282  
1283 **Figure 5.** MJO EWR diagnostics – wavenumber-frequency power spectra – from (a) GPCP v1.3  
1284 (Huffman et al., 2001) and (b) IPSL-CM5B-LR model of CMIP5. The EWR is defined as the ratio  
1285 of eastward power (averaged in the box on the right) to westward power (averaged in the box  
1286 on the left) from the 2-dimensional wavenumber-frequency power spectra of daily 10°S–10°N  
1287 averaged precipitation in November to April (shaded,  $\text{mm}^2 \text{day}^{-2}$ ). Power spectra are calculated  
1288 for each year and then averaged over all years of data. The units of power spectra for the  
1289 precipitation is  $\text{mm}^2 \text{day}^{-2}$  per frequency interval per wavenumber interval.



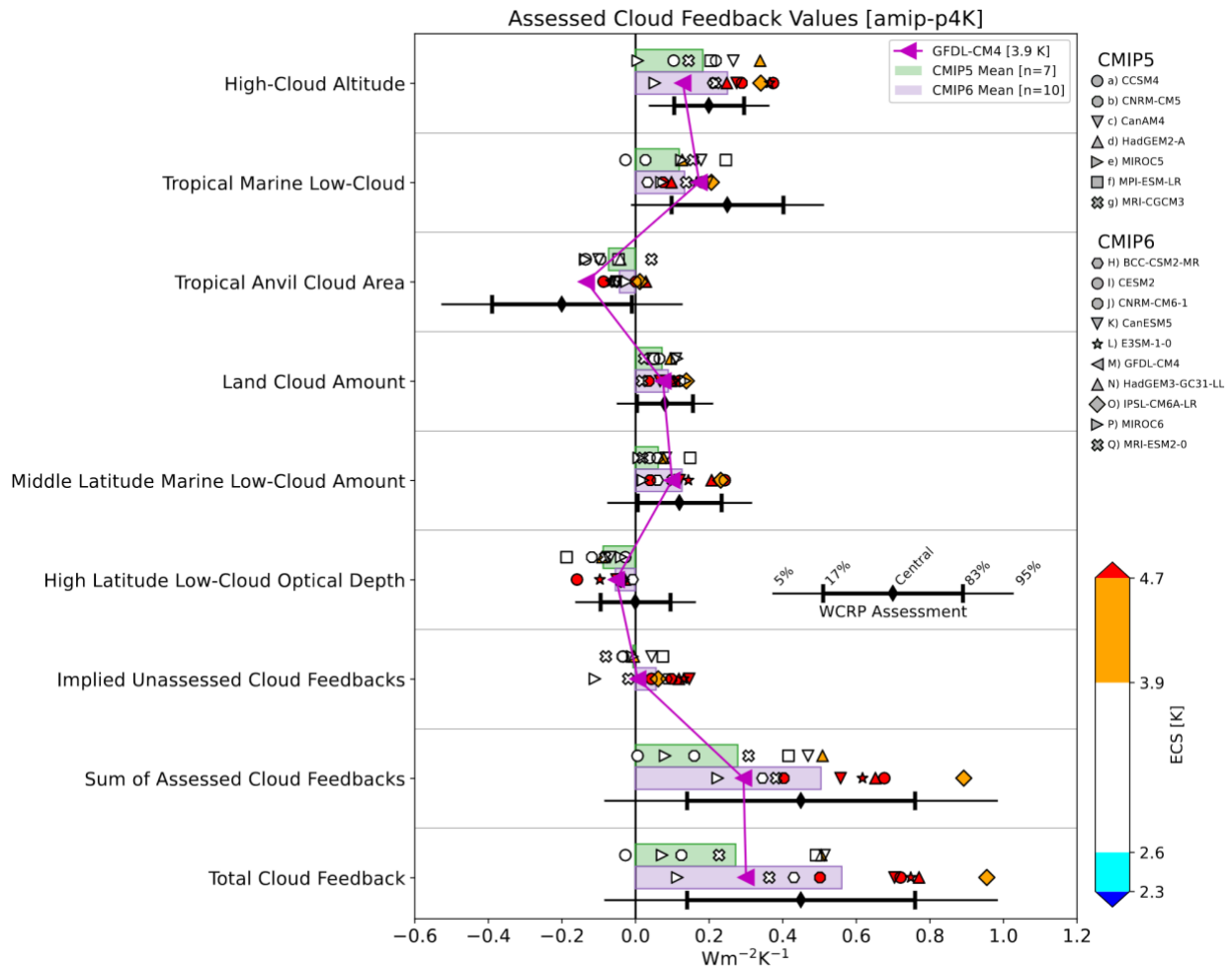
1290  
 1291  
 1292  
 1293  
 1294  
 1295  
 1296  
 1297  
 1298  
 1299  
 1300

**Figure 6.** MJO East-West Power Ratio (EWR, *unitless*) from CMIP5 and CMIP6 models, models in two different groups (CMIP5: blue, CMIP6: orange) are sorted by the value of the metric and compared to two observation datasets (purple, GPCP v1.2 and v1.3; Huffman et al., 2001). Horizontal dashed lines indicate EWR from the default primary reference observation (i.e., GPCP v1.3, black), averages of CMIP5 and CMIP6 models. The interactive plot is available at <https://pcmdi.llnl.gov/research/metrics/mjo/> where the horizontal axis can be resorted by CMIP group or model names as well. Hover mouse over boxes will show tooltips for metric values and a preview of dive-down plots that are shown in Figure 5.



1301  
 1302 **Figure 7.** Demonstration of the monsoon metrics obtained from observation datasets (GPCP  
 1303 v1.3 and CMORPH v1.0 (Joyce et al., 2004; Xie et al., 2017)) and a CMIP6 model's Historical  
 1304 simulation conducted using CNRM-CM6-1. The results are obtained for monsoon regions: All-  
 1305 India Rainfall (AIR), Sahel, Gulf of Guinea (GoG), North American Monsoon (NAM), South  
 1306 American Monsoon (SAM), and Northern Australia (AUS). The regions are defined in Sperber  
 1307 and Annamalai (2014). Metrics for onset (On), Duration (Du), and Decay (De) derived as  
 1308 differences to the default observation (GPCP v1.3) in pentad indices (observation minus model)  
 1309 are shown at lower right of each panel. Pentad indices for onset and decay of each region are  
 1310 also shown as vertical lines.

1311

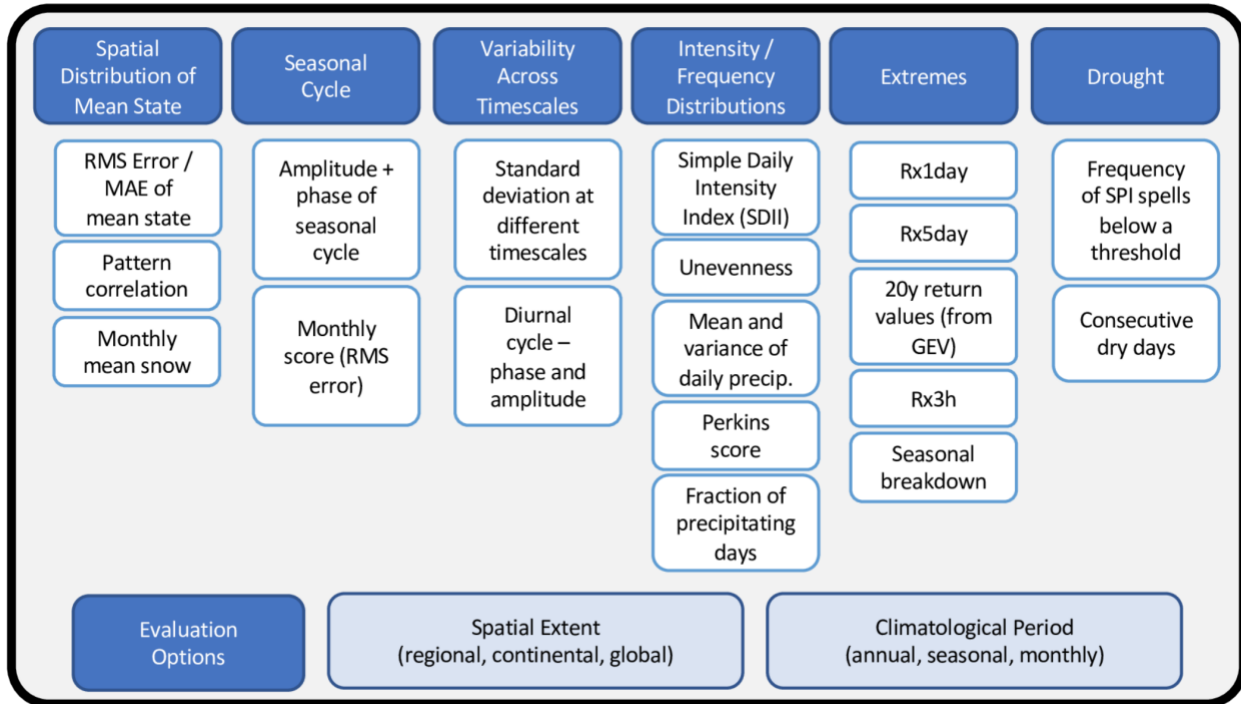


1312  
 1313  
 1314  
 1315  
 1316  
 1317  
 1318

**Figure 8.** Cloud feedback components estimated in amip-p4K simulations from CMIP5 and CMIP6 models. Symbols indicate individual model values, while horizontal bars indicate multi-model means. Each model is color-coded by its ECS, with color boundaries corresponding to the likely and very likely ranges of ECS as determined in Sherwood et al (2020). Each component's expert-assessed likely and very likely confidence intervals are indicated with black error bars. An illustrative model (GFDL-CM4) is highlighted.



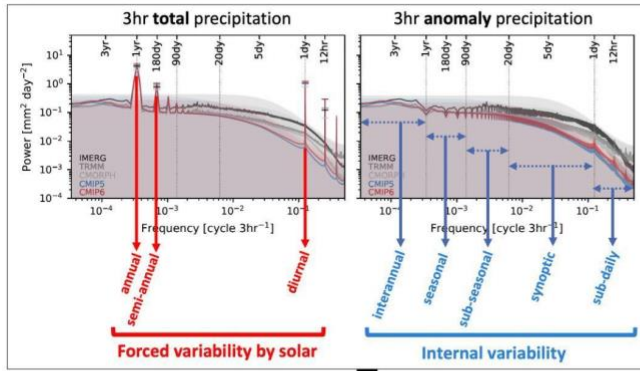
1319



1320  
1321  
1322  
1323  
1324  
1325  
1326

**Figure 9.** Proposed suite of baseline metrics for simulated precipitation benchmarking (figure reprinted from workshop report; US DOE, 2020).

(a) Power spectra (Tropics)

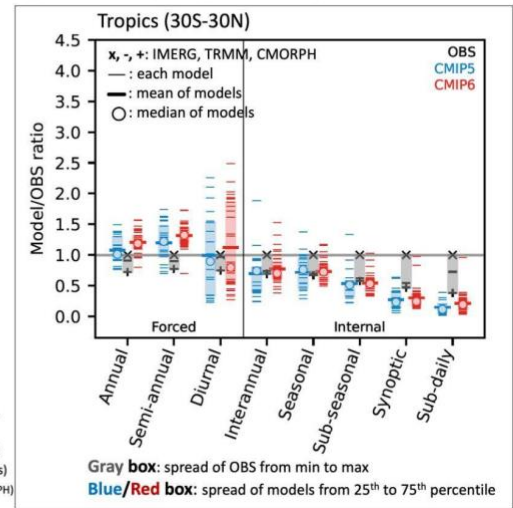


$$\text{Metric} = P_{\text{MODEL}}/P_{\text{OBS}}$$

P: selected or band-averaged power

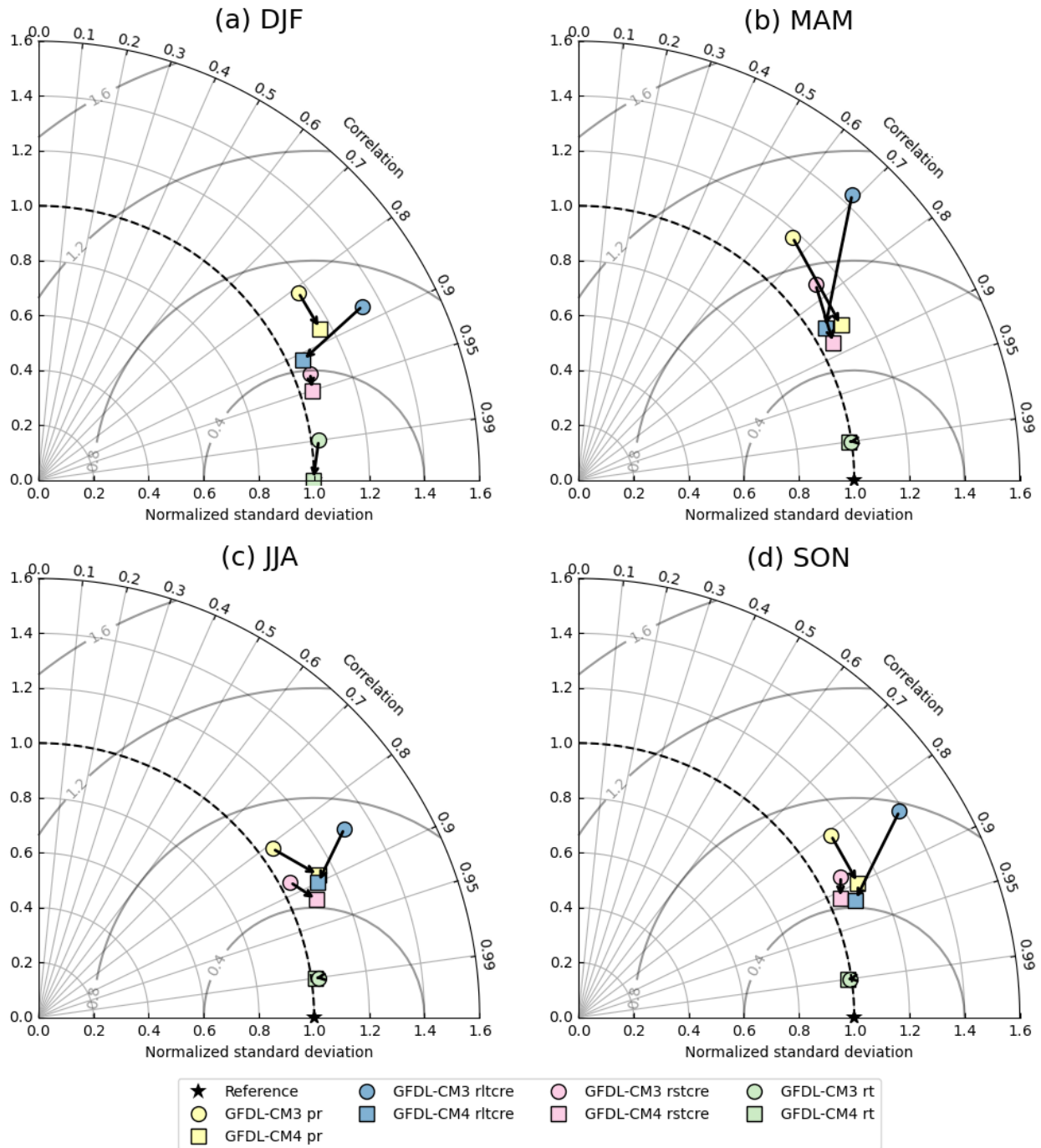
21 CMIP5 (53 realizations)  
33 CMIP6 (143 realizations)  
3 OBS (IMERG, TRMM, CMORPH)

(b) Metric for precip variability across timescales



1327  
1328  
1329  
1330  
1331  
1332  
1333  
1334  
1335  
1336  
1337  
1338  
1339  
1340  
1341

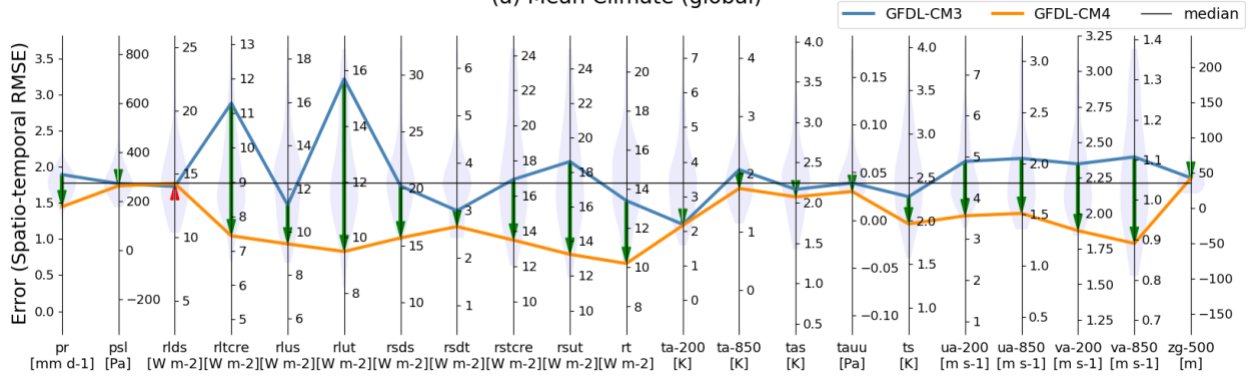
**Figure 10.** Example (a) an underlying diagnostic and (b) its resulting metrics for precipitation variability across timescales. (a) Power spectra of 3-hourly total (left) and anomaly (right) precipitation from IMERG (black), TRMM (gray), CMORPH (silver), CMIP5 (blue), and CMIP6 (red) averaged over the tropics (30°S-30°N). The colored shading indicates the 95% confidence interval for each observational product and for the CMIP5 and CMIP6 means. (b) Metrics for forced and internal precipitation variability based on power spectra. The reference observational product displayed is GPM IMERG (Huffman et al., 2015). The gray boxes represent the spread of the three observational products (“X” for IMERG, “-” for TRMM, and “+” for CMORPH) from the minimum to maximum values. Blue and red boxes indicate the 25th to the 75th percentile of CMIP models as a measure of spread. Individual models are shown as thin dashes, the multimodel mean as a thick dash, and the multimodel median as an open circle. Details for the diagnostics and metrics are described in Ahn et al. (2022).



1342  
 1343  
 1344  
 1345  
 1346  
 1347  
 1348

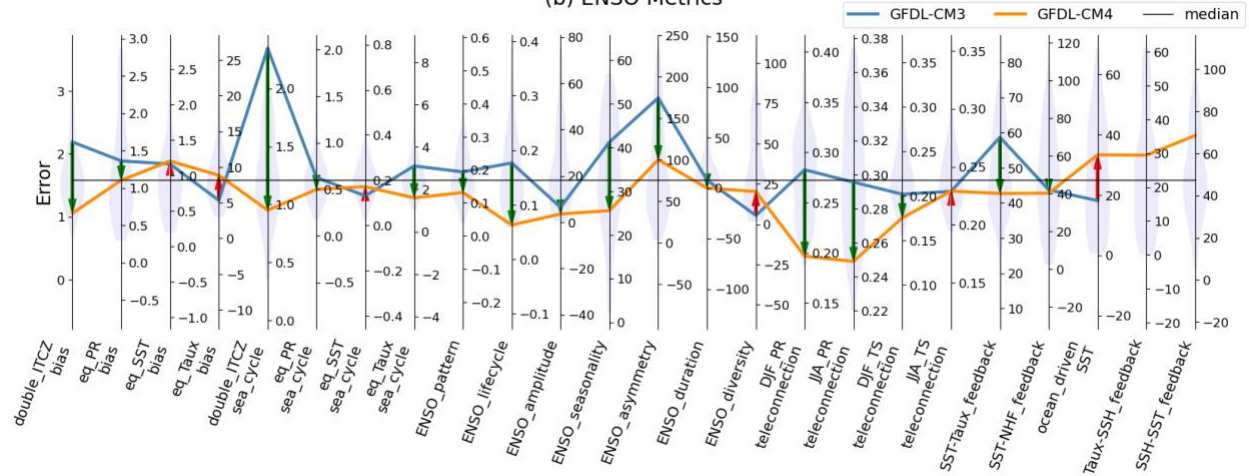
**Figure 11.** Taylor Diagram contrasting performance of an ESM in their two different versions (i.e., GFDL-CM3 from CMIP5 and GFDL-CM4 from CMIP6) in its Historical simulation for multiple variables (precipitation [pr], longwave cloud radiative effect [rltcre], shortwave cloud radiative effect [rstcre], and total radiation flux [rt]) in their climatology over the globe for (a) DJF, (b) MAM, (c) JJA and (d) SON seasons. The arrow is directed toward the newer version of the model from the older version (i.e., GFDL-CM3 → GFDL-CM4).

(a) Mean Climate (global)



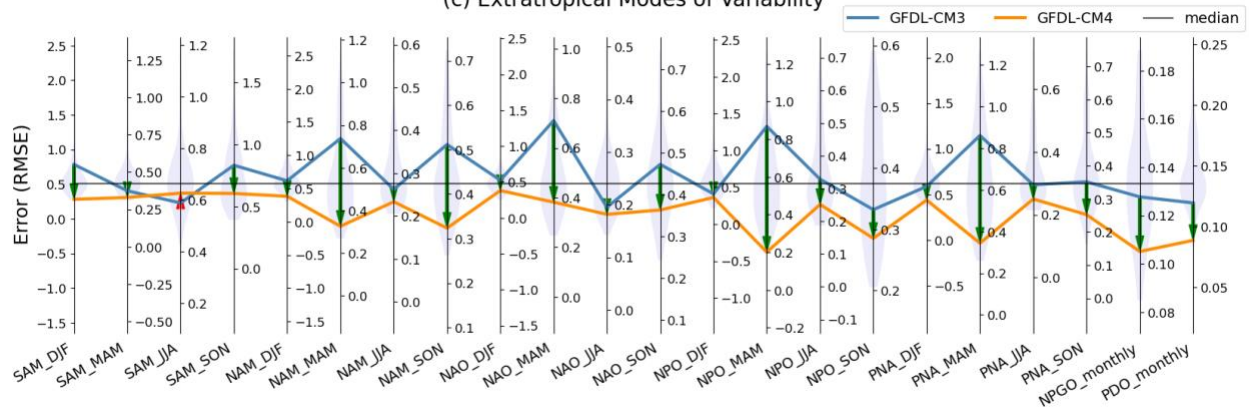
1349

(b) ENSO Metrics



1350

(c) Extratropical Modes of Variability



1351

1352

1353

1354

1355

1356

1357

1358

1359

1360

**Figure 12.** Parallel Coordinate Plot contrasting performance of two different versions of the GFDL model (i.e., GFDL-CM3 from CMIP5 and GFDL-CM4 from CMIP6) in their Historical experiment for errors from (a) mean climate, (b) ENSO, and (c) extratropical modes of variability. Improvement (degradation) in the later version of the model is highlighted as a downward green (upward red) arrow between lines. Middle of each vertical axis is set to the median of the group of benchmarking models (i.e., CMIP5 and CMIP6), with the axis range stretched to maximum distance to either minimum or maximum from the median for visual consistency. The inter-model distributions of model performance are shown as shaded violin plots along each vertical axis.